Computers and Geotechnics 80 (2016) 199–214

Contents lists available at ScienceDirect

Computers and Geotechnics

journal homepage: www.elsevier.com/locate/compgeo

Research Paper

Effect of rubber size on the behaviour of sand-rubber mixtures: A numerical investigation

J.C. Lopera Perez [a], C.Y. Kwok [a,*], K. Senetakis [b]

[a] Department of Civil Engineering, The University of Hong Kong, Haking Wong Building, Pokfulam Road, Hong Kong
[b] School of Civil and Environmental Engineering, University of New South Wales, Sydney NSW 2052, Australia

ARTICLE INFO

Article history:
Received 4 November 2015
Received in revised form 13 June 2016
Accepted 11 July 2016

Keywords:
Sand-rubber mixtures
Shear modulus
Stiffness
Discrete-element modelling
Micro-mechanics
Fabric/structure of soils
Particle-scale behaviour

ABSTRACT

Mixtures of sand and rubber particles were simulated using DEM. Rubber content varied from 0% to 50%. The numerical samples were sheared in the range of 10^{-5}–10^{-2}% of ε_1. The macro-mechanical response changed depending on the size of rubber particles. As the size of the rubber particles increased, the effect of rubber in the internal structure was attenuated, facilitating the force transmission through sand-sand contacts. Largest rubber particles showed the most advantageous mechanical behaviour. Nevertheless, the selection of both rubber size and content will depend on the intended purpose of use for the mixtures.

1. Introduction

The employment of granulated rubber or waste tire shreds as a new geo-material or in the form of mixtures with soil has become a popular approach in ground–improvement [5,11,63]. The rubber is seen to reinforce sand meanwhile it still keeps its lightweight ability. The application of it could certainly be advantageous in engineering projects such as: (i) reduction of lateral earth pressures on retaining walls [18,24,25,27]; (ii) reduction of settlements for embankments [6,10,12]; (iii) providing filter layers for drainage in landfills [47]; and (iv) providing damping to foundations and for liquefaction mitigation purposes [23,33,37,42,43,51–53,57].

Scrap tyres are shredded to smaller sizes for use in various applications, with the actual size, ranging from cuts (>300 mm), shred (50–300 mm), chips (10–50 mm) to powder (<1 mm), depending upon the intended use. At current practice, the determination of the rubber size is mainly based on the availability and the cost of production. Therefore, the effect of rubber size on the behaviour of sand-rubber mixtures has been of interest. Size ratio of rubber to sand particles has been studied in the range of 0.25 [28] to more than 100 [68]. The size of rubber particles has an important effect on the mechanical response of the mixtures that can result either in decay in strength and maximum shear modulus [1,28,29,57] or in increase in strength and maximum shear modulus [26]. Evans and Valdes [15] carried out numerical one dimensional (1-D) compression tests on sand-rubber mixtures to study the effect of rubber fraction and size ratios of particles on the force percolation and the strain dependent evolution of strength. Numerical simulations reported by Lee et al. [30] also corresponded to 1-D compression tests, but only a size ratio of rubber to sand particles of 1.0 was considered in that work with a particular focus on the effect of rubber content on the overall fabric of the samples. Special attention has also been paid to other important parameters, such as the shear modulus measured at very small strains where pure elasticity dominates the behaviour of the mixtures (less than 0.001%) and at small to medium strains where the stiffness already starts to degrade (for example in the range of 0.001–0.1% of shear strain). The small-strain and the small to medium strain shear moduli are usually required in advanced modelling for the accurate prediction of ground deformations [60]. A number of experimental works have been carried out ranging from very small strains up to strains greater than 20% [1,13,14,26,28,29,32,40,52,57]. However, numerical investigations on rubber and sand mixtures have been mainly focusing on medium to large strains up to 20% [30,64].

In this study, mixtures of rubber and sand particles are simulated in three dimensional triaxial constant volume tests by

* Corresponding author.
E-mail address: fiona.kwok@hku.hk (C.Y. Kwok).

http://dx.doi.org/10.1016/j.compgeo.2016.07.005
0266-352X/

Nomenclature

a_n	normal contact force anisotropy
d	particle diameter
G^p	particle shear modulus
G	elastic secant shear modulus
G_{max}	maximum elastic secant shear modulus
I	inertial number
p'	mean effective stress
p'_0	mean effective stress after isotropic compression
q	deviatoric stress $q = \sigma'_1 - \sigma'_3$
Z_m	mechanical coordination number
$\dot{\varepsilon}$	strain rate
ε_1; ε_2; ε_3	major, intermediate and minor principal strains ($\varepsilon_2 = \varepsilon_3$)
ε_q	shear strain $\varepsilon_q = 2/3(\varepsilon_1 - \varepsilon_3)$
μ	inter-particle friction coefficient
v	particle Poisson's ratio
ρ	particle density
σ'_1; σ'_2; σ'_3	major, intermediate and minor principal stresses ($\sigma'_2 = \sigma'_3$)
$(\Phi_1 - \Phi_3)$	deviatoric fabric

employing the discrete element method (DEM) to investigate the effects of rubber content and the relative size of rubber and sand particles at small strains. As noted by Lee et al. [30], the response of granular materials at different strain levels would underlie a different response at the micro-mechanical level. The purpose of this contribution is to explore the micro-mechanics that are developed in a range of strains usually experienced by geo-materials, i.e. pre-failure response and in particular to investigate the contribution that is made by each type of contact, i.e. sand-sand, rubber-sand or rubber-rubber to both the micro and macro-mechanical responses. Sand particles are modelled as rigid particles with high stiffness, whereas rubber particles are modelled as soft particles having low stiffness. Macro- and micro-scale responses of sand-rubber mixtures will be explored. The DEM simulations allow the tracking of the particle contacts and the distribution and magnitude of the forces at all test stages, which is not feasible in laboratory experiments.

2. The discrete element method

The simulations presented in this study used the DEM proposed by Cundall and Strack [8]. The calculation cycle applies a force-displacement law to the particles and updates the particle positions by the Newton's second law. A soft contact approach is used where particles are treated as rigid but allow overlapping among each other at a contact point occurring over a small area. Normal and tangential forces generated at contacts are calculated respectively as $f_n = k_n\delta_n$ and $\Delta f_t = k_s\Delta\delta_s$ where k_n and k_t are the normal and tangential stiffness, respectively, δ_n is the contact overlap and $\Delta\delta_s$ is the tangential displacement increment. The maximum tangential force allowed is given by $f_{t\ max} = \mu\ f_n$ with μ being the interparticle-friction coefficient. k_n and k_t are calculated using the Hertz-Mindlin contact model as: $k_n = \frac{2G^p}{1-\nu}\widetilde{R}^{1/2}\delta_n^{1/2}$ and $k_t = \frac{4G^p}{2-\nu}\widetilde{R}^{1/2}\delta_n^{1/2}$, where G^p is the particle shear modulus, ν the particle Poisson's ratio and R is the equivalent radius in between two particles in contact i and j obtained as: $\widetilde{R} = \frac{R_iR_j}{R_i+R_j}$. This contact model uses an approximation of the theory of Mindlin and Deresiewicz [35] where the contact model excludes the continuous nonlinearity in shear while only the initial shear modulus is used. This contact model has been widely adopted in DEM simulations which have successfully captured typical soil behaviour characteristics [2,20,61,66].

The use of a local damping facilitates the kinetic energy dissipation allowing the system reducing the number of calculation cycles required for the system to reach equilibrium. The damping force is calculated as $F_d = \mathrm{d}|F_u| \pm (V)$, where d is the local damping ratio. It is proportional to the unbalanced force F_u and applied opposite to the velocity direction V.

The simulations shown in this study were carried out in the open-source code LAMMPS (Large-scale Atomic/Molecular Massively Simulator) [44] which is a classical molecular dynamics (MD) code capable of simulating soft matter and coarse-grained systems. LAMMPS can run on single or in parallel using MPI techniques allowing its use on massively-parallel high-performance computers. The MD method is algorithmically similar to DEM and a number of implementations were made onto LAMMPS to allow the simulations of granular assemblies by using DEM. Details of this modified version of LAMMPS can be found in Huang [22]. Additional implementations include the possibility of simulating a granular system composed of two different materials where, in the case of a contact shared by the two materials, the shear modulus and Poisson's ratio is taken as the average of the two materials. Besides, the tangential force arouse from a contact between the two different materials is limited by the minimum inter-particle friction coefficient among the materials.

DEM employed in this study can capture part of the behaviour of discrete materials such as soils, and can provide useful information associated with micro-quantities. It should be noted that in this study particles are modelled as perfect spheres with which the effect of the particle shape on the response of granular materials is not captured [65]. Nevertheless, DEM has proven to be an appropriate tool for modelling the different phenomena that characterize granular systems as was summarized by O'Sullivan and Bray [39]. In this regard, a careful calibration of the system was conducted, in particular for the pure sand (assembly of stiff grains) and the pure rubber (assembly of soft grains) with respect to the small-strain stiffness of the samples based on literature data derived from resonant column tests.

3. Numerical simulations

The particle size distribution (PSD) used for the simulated sand is plotted in Fig. 1, which is representative of a uniform sand of fluvial origin tested by Anastasiadis et al. [1]. Rubber particles were created following three different PSD parallel to the sand PSD, having ratios of mean size of rubber to mean size of sand (D_{50R}/D_{50S}) of 1.0, 2.5 and 5.0, as seen in Fig. 1. A total of 15 mixtures were prepared, 5 for each D_{50R}/D_{50S}, with rubber contents varying from 10% to 50% by mixture weight, in increments of 10%. Views of the numerical samples for the clean sand and the mixtures at 100 kPa of isotropic confining pressure are also included in Fig. 1.

Each sample consisted of a total number of particles ranging from 10,184 to 20,692. Particles were placed initially as non-contacting spherical particles, and enclosed within a cuboidal periodic cell to avoid boundary effects [21,62]. The stresses within the periodic cell were determined from the stress tensor as

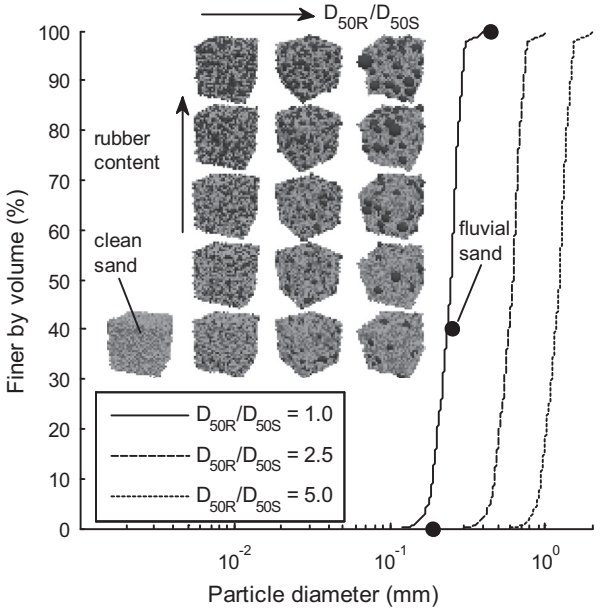

Fig. 1. Particle size distribution of numerical samples.

$\bar{\sigma}_{ij} = \frac{1}{V}\sum_{1}^{N_c} l_i^c f_j^c$ where $\bar{\sigma}_{ij}$ is the stress tensor, V is the volume of the periodic cell, N_c is the total number of contacts, l_i^c and f_j^c are the branch vector and the inter-particle contact force corresponding to contact c respectively [3,45].

In the simplified Hertz-Mindlin contact model, sand particles were assigned a particle Poisson's ratio (ν) of 0.12 following the properties of quartz [59] and a density (ρ) of 2650 kg/m^3. Input parameters for rubber particles include a ν of 0.45 which is consistent with their very small volume compressibility [4] and ρ of 1100 kg/m^3. For the simulated sand and rubber, the particle shear modulus (G^p) was calibrated, yielding in a contact stiffness that allowed an amount of stress at certain deformation within a dense sample that would match the real G_{max}. Initially, the G_{max} of a clean uniform fluvial sand and granulated rubber studied by Anastasiadis et al. [1] and Senetakis et al. [53] was calibrated as shown in Fig. 2a, in which G_{max} is plotted against p' and Fig. 2b showing G_{max} against the major principal strain (ε_1). G_{max} is calculated from $G = (2/3)q/\varepsilon_q$, where q is the deviatoric stress and ε_q is the shear strain calculated as the difference between the major and minor principal strain ($\varepsilon_1 - \varepsilon_3$), and was obtained at a strain magnitude of 10^{-4}%. Different values of particle shear modulus ranging from 2.5 MPa to 29 GPa were used. For the simulated sand, in each set of particle shear modulus, different initial coefficients of friction were used to create samples with different densities in order to investigate its effect on G_{max} while for the simulated rubber μ was set to 1.0. As the initial void ratio increased, lower values of G_{max} were attained, and this dependence on initial void ratio increased as G^p decreased. A seen in Fig. 2, a value of G_s^p = 8 GPa for the simulated sand and G_r^p = 12 MPa resulted in good agreement with the laboratory data, where G_{max} and its degradation with strain were matched. A small local damping coefficient with a value of 0.1 was used for all simulations, which does not affect the mechanical response of the system. Gravity is inactive during the simulations in order that the stress distribution is uniform within the sample, besides it permits an easier identification of particles not contributing to the stress transmission within the sample. All simulations were run on a high-performance cluster using a stable time step of 5.3 ns.

During the isotropic compression stage, the periodic cell was deformed until mean effective stresses (p'_0) of 50 kPa, 100 kPa and 200 kPa were reached. In order to avoid excessive overlaps that could lead to negative void ratios, p'_0 was kept to a relatively low value. Sand particles were assigned an inter-particle friction coefficient (μ) of 0.01 while rubber particles were assigned a μ of 1.0 during the isotropic compression stage. After the samples reached the target p'_0 the system was subjected to numerical cycling, ensuring that both p' and the number of contacts remained constant, indicating equilibrium. The same isotropic compression stage procedure was applied to all D_{50R}/D_{50S} ratios considered in this study. Low void ratios were attained for the case of D_{50R}/D_{50S} = 5.0. For these mixtures, any voids formed by rubber particles

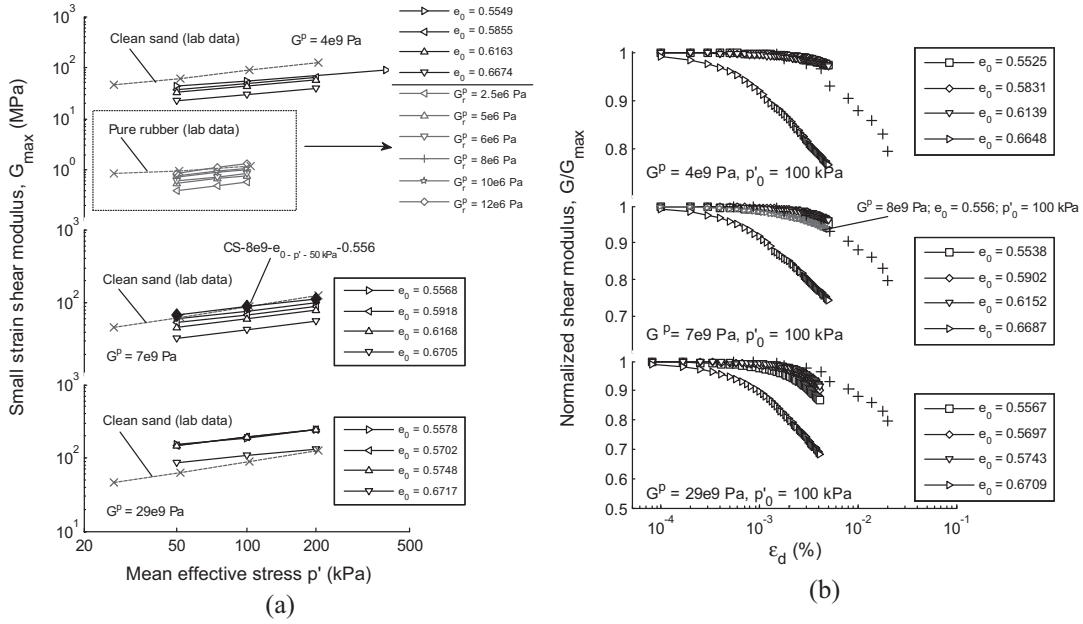

Fig. 2. Calibration of simulated sand and rubber shear modulus to lab data, (a) small strain shear modulus against mean effective stress and (b) normalized shear modulus against shear strain.

Table 1
List of tests conducted.

Set test ID	$e_{0(p'=50\ kPa)}$	p'_0 (kPa)	D_{50R}/D_{50S}	Rubber content (%)	No. sand particles	No. rubber particles	Size of numerical specimens (mm) p'_0 = 50 kPa (100 kPa for pure rubber)
CS-p'_0	0.5560	50, 100, 200	–	–	10184	0	4.591 × 4.590 × 4.627
M10-1:1-p'_0	0.5669	50, 100, 200	1	10	8212	1972	4.634 × 4.614 × 4.592
M20-1:1-p'_0	0.5965	50, 100, 200		20	6916	3268	4.658 × 4.642 × 4.627
M30-1:1-p'_0	0.6176	50, 100, 200		30	5945	4239	4.698 × 4.627 × 4.664
M40-1:1-p'_0	0.6316	50–100–200		40	5201	4983	4.724 × 4.669 × 4.636
M50-1:1-p'_0	0.6390	50–100–200		50	4689	5495	4.712 × 4.651 × 4.687
M10-2.5:1-p'_0	0.5162	50, 100, 200	2.5	10	20363	329	6.182 × 6.196 × 6.137
M20-2.5:1-p'_0	0.4703	50, 100, 200		20	18116	521	6.233 × 6.266 × 6.180
M30-2.5:1-p'_0	0.4715	50, 100, 200		30	15863	717	6.297 × 6.255 × 6.224
M40-2.5:1-p'_0	0.4644	50–100, 200		40	13541	815	6.205 × 6.113 × 6.285
M50-2.5:1-p'_0	0.4604	50–100, 200		50	11358	869	6.108 × 6.017 × 6.058
M10-5:1-p'_0	0.4830	50, 100, 200	5	10	20401	42	6.157 × 6.070 × 6.133
M20-5:1-p'_0	0.4308	50, 100, 200		20	18153	67	6.277 × 6.159 × 6.057
M30-5:1-p'_0	0.3988	50, 100, 200		30	15767	101	6.205 × 6.001 × 6.277
M40-5:1-p'_0	0.3695	50, 100, 200		40	13613	105	6.360 × 5.899 × 5.940
M50-5:1-p'_0	0.3490	50, 100, 200		50	11374	108	5.688 × 6.112 × 5.888
M100-p'_0	0.5089	100	–	100	0	10184	4.641 × 4.626 × 4.634

would be filled by smaller sand particles. Similar void ratios have been reported from DEM studies of for example particle size distribution [36,58].

After the completion of the isotropic compression stage, sand particles were assigned an inter-particle friction coefficient (μ) of 0.25 [20,21,54–56] while rubber particles were given a μ of 1.0 [15,30,50,64]. The particle shear modulus assigned to the sand was G_s^p = 8e9 Pa while for rubber G_r^p = 12e6 Pa. The numerical samples were sheared in compression in a strain–rate controlled manner under constant volume (CV) conditions covering from the very small to the relatively medium strain ranges. The incremental axial deformation of the periodic cell was set to $d\varepsilon$ = 1e−8. The strain rate ($\dot{\varepsilon}$) used for all tests was calculated by dividing $d\varepsilon$ by the time-step. The inertial number, defined as $I = \dot{\varepsilon} d\sqrt{\rho/p'}$, where $\dot{\varepsilon}$ is the shear rate, d is the mean size of grains in the assembly, ρ is the grain density, and p' is the mean effective stress, was used to ensure quasi-steady conditions during the shearing process, where a limit of $I \leqslant$ 1e−3 would be sufficient to maintain quasi-steady conditions [9,31,34]. For the particular study, the focus was on stiffness from very small to medium strains and the micro-quantities that may explain the behaviour of the mixtures, thus the decision to perform undrained tests instead of drained tests, would not affect the interpretations and outcomes of this work. Besides, it has been shown that in DEM, the conduction of tests both under drained and constant volume conditions capture the salient characteristics of soil behaviour [16,17]. Table 1 summarizes the simulations carried out in this study, where samples are labelled as CS-XX for Clean Sand, with XX indicating the initial p'_0, and MC-R-XX for sand-rubber mixtures, with C indicating the content of rubber in percentage, R giving the D_{50R}/D_{50S}, and similarly, XX indicating the initial p'_0.

4. Results

4.1. Macro-scale response of sand-rubber mixtures

The deviatoric stress is plotted against ε_1 in Fig. 3(a) for samples sheared from a p'_0 of 50 kPa; each subfigure relates a different D_{50R}/D_{50S}. For the case of D_{50R}/D_{50S} = 1.0, a significant lower rate of increase of q is observed as rubber content increases. A similar trend is observed for D_{50R}/D_{50S} = 2.5, however, the rate of increase of q is less affected by the increase of rubber content in this case. The clean sand achieved the highest q for D_{50R}/D_{50S} = 1.0 and 2.5 cases, however this is not true for the case of D_{50R}/D_{50S} = 5.0 and no easily noticeable trends can be observed.

Fig. 3(b) illustrates the response on the stress plane q-p' for all samples sheared from a p'_0 of 50 kPa with each subfigure relating a different D_{50R}/D_{50S}. A reduction in p' would indicate a tendency of the numerical sample to contract, whereas an increase would indicate a tendency to dilate. The trend of decreasing p' since the sample is sheared undrained would imply that under drained conditions it should exhibit contraction behaviour, i.e. decrease of volume. Conversely, with p' increasing under undrained conditions, if it were under drained conditions, then it would show dilation in its behaviour, i.e. increase in volume. Only the CS-50 and M50-1:1-50 tests displayed a clear contractive response. The sample with 0% of rubber content can be taken as a dense sample; for dense samples it is possible to initially contract (decrease in p') and then dilate (increase in p') with a phase transformation point. In the range of strains considered in the simulations, the point of phase transformation was not reached. However, the contractive response from M50-1:1-50 is mainly due to its looser packing. Up to the strain levels considered, all other samples showed clearly a dilative response, where larger p' were found as D_{50R}/D_{50S} increased. As soon as rubber particles are added into a sand matrix, a change from contractive to dilative response is observed. This can be related to the increase of the branch vector resulting in higher forces that lead to a higher concentration of mean effective stress.

Fig. 4(a) presents the effect of rubber content on q at different levels of ε_1 for samples sheared from a p'_0 of 50 kPa. As ε_1 increases, any effect that rubber had on q becomes more evident regardless of the ratio D_{50R}/D_{50S}. In the case of D_{50R}/D_{50S} = 1.0, there is always a decrease in q as rubber content increases, while a slight decrease in q is noticeable in samples with D_{50R}/D_{50S} = 2.5 at ε_1 = 1e−4%. This trend becomes clearer at higher levels of ε_1 and at rubber contents greater than 20%. An almost constant value of q is observed for the case of D_{50R}/D_{50S} = 5.0 at ε_1 = 1e−4%. At ε_1 = 1e−3%, the initial increase in q up until a rubber content of 20% becomes more evident, followed by a constant response in the 20–40% range of rubber content, from where a sharper decay in q is appreciated. Regardless of the strain level, tested samples with D_{50R}/D_{50S} = 5.0

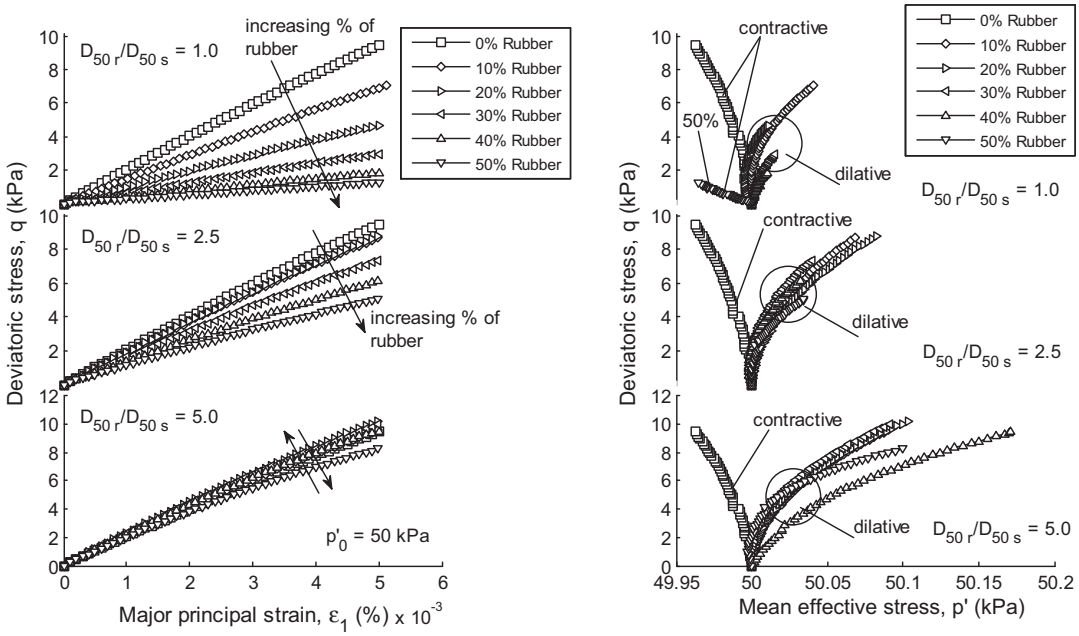

Fig. 3. Stress-strain response for different D_{50R}/D_{50S}. (a) Deviatoric stress against major principal strain and (b) deviatoric stress against mean effective stress.

having either 0% or 50% of rubber content showed almost no difference in q.

The deviatoric stress q is linked to the small-strain shear modulus (G_{max}). Fig. 4(b) contains the small-strain shear modulus (G_{max}) for all tests conducted, calculated at a value of ε_1 = 1e−4%. The trend of G_{max} with rubber content from the numerical simulations for mixtures with a size of rubber grains equal to that of the sand, closely matched that from the laboratory experiments reported by Anastasiadis et al. [1]. Numerical results from mixtures with D_{50R}/D_{50S} = 5.0 follow a similar trend of that found by Kim and Santamarina [26] where there is an initial increase in stiffness up to a rubber content of 20% followed by a continuous drop in stiffness. Although Kim and Santamarina [26] used a different sand and mixtures with a size ratio of D_{50R}/D_{50S} = 10 (rubber content was measured by volume instead of weight), as noted by Youwai and Bergado [67] when D_{50R}/D_{50S} > 6 size effects are negligible, thus making it possible to relate the two trends.

The inclusion of rubber particles with D_{50R}/D_{50S} of 1.0 into a matrix of sand results in a clear exponential decay in G_{max} with an increase in rubber content. As rubber content increases the

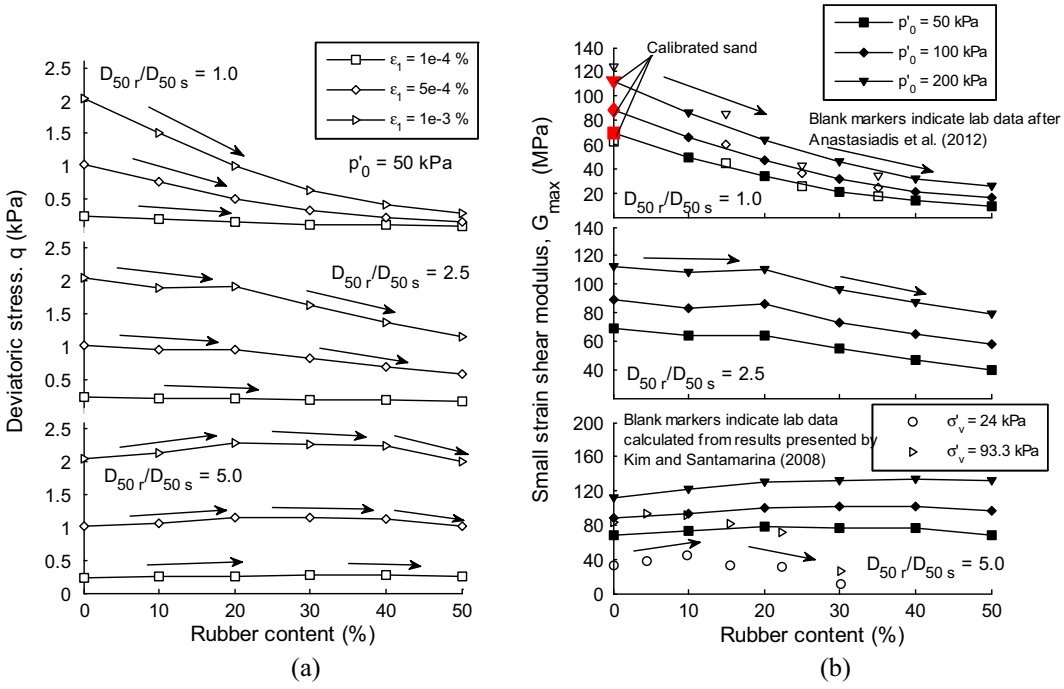

Fig. 4. (a) Deviatoric stress at different levels of major principal strain and (b) small strain shear modulus at different levels p'_0, against rubber content for different D_{50R}/D_{50S}. Lab data from Kim and Santamarina [26] at different vertical effective stress (σ'_v) levels.

values of G_{max} for the p'_0 considered start to converge. For a ratio D_{50R}/D_{50S} equal to 2.5, the trend of decreasing G_{max} is more pronounced at greater percentages of rubber. G_{max} appears almost constant up to a rubber content of 20% beyond which, a linear decay in shear modulus takes place as rubber content increases. The decay in G_{max} appears to be parallel among the different p'_0. Samples with a D_{50R}/D_{50S} ratio of 5.0 present a more complex response. G_{max} increases linearly as rubber content increases up to 20%. For rubber contents in the range of 20–40%, G_{max} remains constant, and a decrease in G_{max} takes place when rubber content is more than 40%.

The underlined tests from Table 1 refer to additional simulations carried out under conventional drained conditions (constant σ'_3) sheared to larger strains ($\varepsilon_1 \sim 20\%$). Laboratory data has been collected from Youwai and Bergado [67], Zornberg et al. [68], Mashiri et al. [32] and Bolton [7] in order to compare the trends on the mobilized friction angle (ϕ) and the dilatancy angle ($\phi_{max} - \phi_{crit}$) with the outcomes from the numerical simulations. Fig. 5 serves to highlight the ability of the numerical simulations to qualitatively match the response from laboratory tests. In Fig. 5a, q at failure is plotted against rubber content for different lab data and for the numerical simulations. q is seen to increase with rubber content up to a value in the range of 20–40%. The initial increase in q with increase in rubber content is well captured. Besides, the effect of rubber size can also be observed. Fig. 5b plots the dilatancy angles for a range of sand taken from Bolton [7] where the dilatancy angle for the numerical simulations are seen to fall in the range of those from laboratory experiments under similar levels of confining pressures. It should be noticed that for the numerical simulations, as p' increases the initial void ratio decreases and thus larger dilatancy angles are evident.

As discussed above, the calibration stage led to input parameters for the numerical simulations, that allowed G_{max} and its degradation to be successfully captured quantitatively and qualitatively. It should be under small strains, there almost no change in number of contacts and in the structure of the contact network. This means, that no re-accommodation and movements of particles take place and thus factors such as shape do not affect the quantitative response of the assembly. However, when samples are sheared to larger strains ($\varepsilon_1 > 1\%$), changes in the contact structure inevitably take place and thus re-arranging and movement of particles occurs within the sample. In this case, shape of particles plays a vital role if the quantitative matching of data is desired. This is a limitation of DEM when considering spherical particles. Nevertheless, it is possible to match qualitatively the laboratory results with the numerical simulations.

4.2. Micro-scale response of sand-rubber mixtures

4.2.1. Coordination number

A particle scale examination of the system response can offer insights into the physical basis of the effect of rubber particle size and percentage of rubber content in the behaviour of sand-rubber mixtures. As a first approach, the number of contacts per particle in the system was quantified by employing the definition of the mechanical coordination number (Z_m), which excludes "rattlers" with zero or one contact [62]. An overall Z_m throughout the shearing stage, considering all contacts, as well as a coordination number for each type of contact (sand-sand, rubber-sand or rubber-rubber) calculated following Minh and Cheng [36] as: $Z^{s-s} = 2C^{s-s}/N^{s-s}$; $Z^{r-s} = 2C^{r-s}/N$ and $Z^{r-r} = 2C^{r-r}/N^r$, where N^s is the number of sand particles, N^r is the number of rubber particles and N is the total number of particles. The coordination number, in laboratory experiments or numerical simulations, is affected, partly by the sample preparation method. However, in this study, the same preparation method was applied for all the simulated sand-rubber mixtures, thus the consistency in sample creation may minimize such effects on the coordination number.

An initial observation is that regardless of the type of contact, rubber content and rubber size, Z_m remains virtually constant in

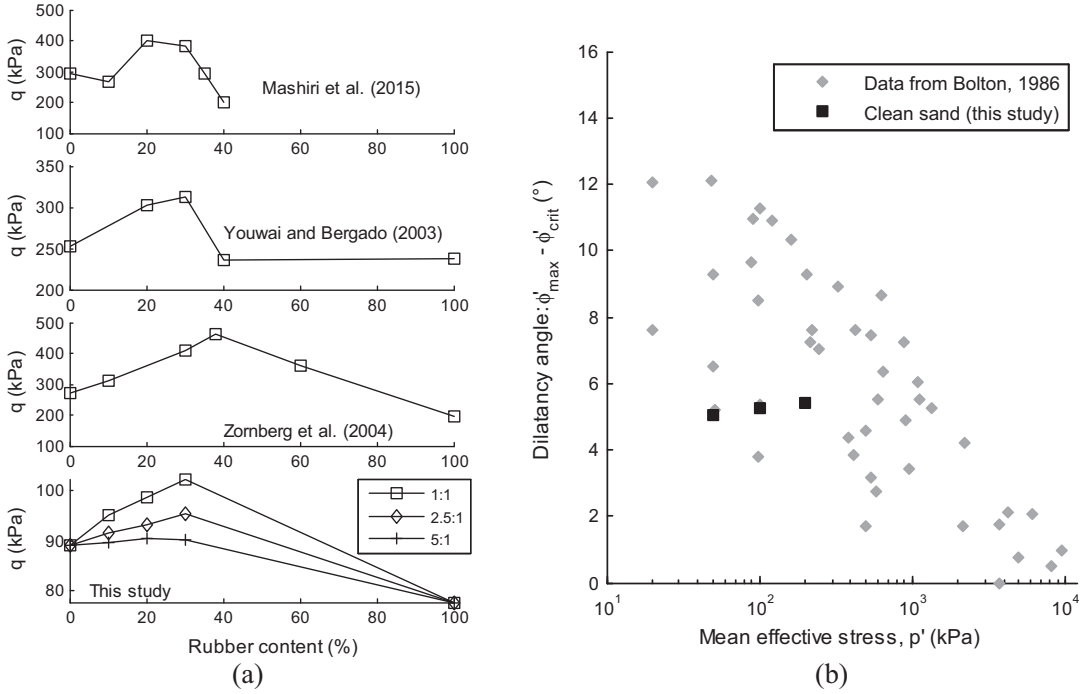

Fig. 5. (a) Deviatoric stress at failure against rubber content from this study and from laboratory data from Youwai and Bergado [67], Zornberg et al. [68] and Mashiri et al. [32]. (b) Dilatancy angle from this study compared from available data from Bolton [7].

the range of small ε_1 considered in this study as seen in Fig. 6. Yet, the values of Z_m present interesting trends depending on the rubber content and size of rubber particles. $Z^{s\text{-}s}$ for all D_{50R}/D_{50S} ratios considered, tends to decrease as rubber content increases, however as D_{50R}/D_{50S} increases the decrease of Z_m becomes less significant. This can be easily understood as the number of rubber particles decreases with the increase of D_{50R}/D_{50S} ratio for a given rubber content. Rubber-rubber contacts present the opposite trend with Z_m increasing as rubber content increases however the maximum $Z^{r\text{-}r}$ decreases as D_{50R}/D_{50S} increases.

$Z^{r\text{-}s}$ presents a clear increase as rubber content increases in the cases of $D_{50R}/D_{50S} = 2.5$ and $D_{50R}/D_{50S} = 5.0$, but for the case of $D_{50R}/D_{50S} = 1.0$ there is an increase in Z_m from 10% to 20% of rubber content from which the coordination number appears to remain constant at a value of $Z_m = 2.5$ up to a rubber content of 50%.

The overall Z_m for all cases of D_{50R}/D_{50S} and rubber content is similar and about 6 as shown in Fig. 7, indicating that all samples regardless of rubber content and size are stable. Nevertheless, the stability of the system is shared by all types of contacts [36], and their contribution does depend on rubber content and size. As expected, sand-sand contacts decreased as rubber content increases, with the rate of decrease being affected by D_{50R}/D_{50S}. The continuous line at $Z_m = 4$ indicates the minimum Z_m required for the stability of a granular system composed of spherical frictional particles [19]. Sand-sand contacts from D_{50R}/D_{50S} of 1.0 attain values of $Z^{s\text{-}s}$ below 4 for rubber content beyond 20%, suggesting that the overall stability of the system begins to depend on rubber involved contacts. In the case of $D_{50R}/D_{50S} = 2.5$, $Z^{s\text{-}s}$ crosses 4 at a rubber content of 30% coinciding with the clear start of decrease in G_{max} seen in Fig. 4(b), while for $D_{50R}/D_{50S} = 5.0$, $Z^{s\text{-}s}$ remained above 4 indicating a sand controlled mixture when the rubber content is up to 50%. Rubber-sand and rubber-rubber contacts present the opposite trend, with increasing $Z^{r\text{-}s}$ and $Z^{r\text{-}r}$ with rubber content. For rubber-sand contacts, as D_{50R}/D_{50S} increases, lower values of $Z^{r\text{-}s}$ are attained. For mixtures with $D_{50R}/D_{50S} = 1$, $Z^{r\text{-}s}$ reach its maximum at a rubber content of 40% where a small decrease is seen at a content of 50% mainly due to the higher number of rubber particles that are present in the system. With the increase of rubber size, lower values of $Z^{r\text{-}s}$ and $Z^{r\text{-}r}$ are obtained for rubber-sand and rubber-rubber at all rubber contents, hindering the participation of these contacts in the overall stability of the system.

4.2.2. Structural anisotropy

While Z_m gives information associated with the packing density at the contact scale, still additional insights are required in terms of contact orientation and biases in force magnitude. In order to meet those needs, a second parameter corresponding to the structural anisotropy (fabric) is employed in the study by using the fabric tensor defined by Satake [49] and presented in Eq. (1).

$$\Phi_{ij} = \frac{1}{N_c}\sum_{1}^{N_c} n_i n_j \tag{1}$$

where N_c is the total number of contacts and n_i is the unit contact normal. The largest, intermediate and smallest eigenvalues of the fabric tensor are denoted as Φ_1, Φ_2 and Φ_3 respectively. The deviatoric fabric, $(\Phi_1\text{-}\Phi_3)$, relates to the degree of structural anisotropy. An increase in $(\Phi_1\text{-}\Phi_3)$ indicates a larger number of contacts aligned parallel to the direction of loading, while low values of $(\Phi_1\text{-}\Phi_3)$ represent an isotropic contact network. An overall Φ_{ij} was obtained taking into account all contacts, and additionally a Φ_{ij} was found for each type of contact, i.e. sand-sand, sand-rubber and rubber-rubber.

Fig. 8 shows the structural anisotropy against ε_d for each type of contact and for different ratios of D_{50R}/D_{50S}. For sand-sand contacts, the results indicated a decrease in $(\Phi_1\text{-}\Phi_3)$ as D_{50R}/D_{50S} increased. For each D_{50R}/D_{50S} ratio, higher values of $(\Phi_1\text{-}\Phi_3)$ are observed as rubber content increases. No clear trend can be appreciated for rubber-sand contacts; however, it is interesting to note that for a D_{50R}/D_{50S} ratio of 2.5, $(\Phi_1\text{-}\Phi_3)$ remains in the order of 10^{-3} regardless of rubber content, indicating an isotropic rubber-sand contact network. There is a general trend for rubber-rubber contacts acting on a D_{50R}/D_{50S} ratio of 1.0 to decrease in $(\Phi_1\text{-}\Phi_3)$, as rubber content increases with $(\Phi_1\text{-}\Phi_3)$ in the order of 10^{-3} at a rubber content of 50%. Considering rubber-rubber contacts for $D_{50R}/D_{50S} = 2.5$, no clear trend is noticed in $(\Phi_1\text{-}\Phi_3)$ with values of it, in general, of the order of 10^{-2}. A decrease in $(\Phi_1\text{-}\Phi_3)$ as rubber content increases is evident for the case of $D_{50R}/D_{50S} = 5.0$, with the highest values of $(\Phi_1\text{-}\Phi_3)$ among all samples reaching the order of 10^{-1}. $(\Phi_1\text{-}\Phi_3)$ remained virtually constant throughout the shearing stage, with the exception of sand-sand contacts acting in a D_{50R}/D_{50S} of 5.0, where an increase in $(\Phi_1\text{-}\Phi_3)$ is observed beyond a strain ε_d of 1e−3%.

A view to Fig. 9 indicates that regardless of content of rubber or D_{50R}/D_{50S}, all samples remain overall isotropic, with values of

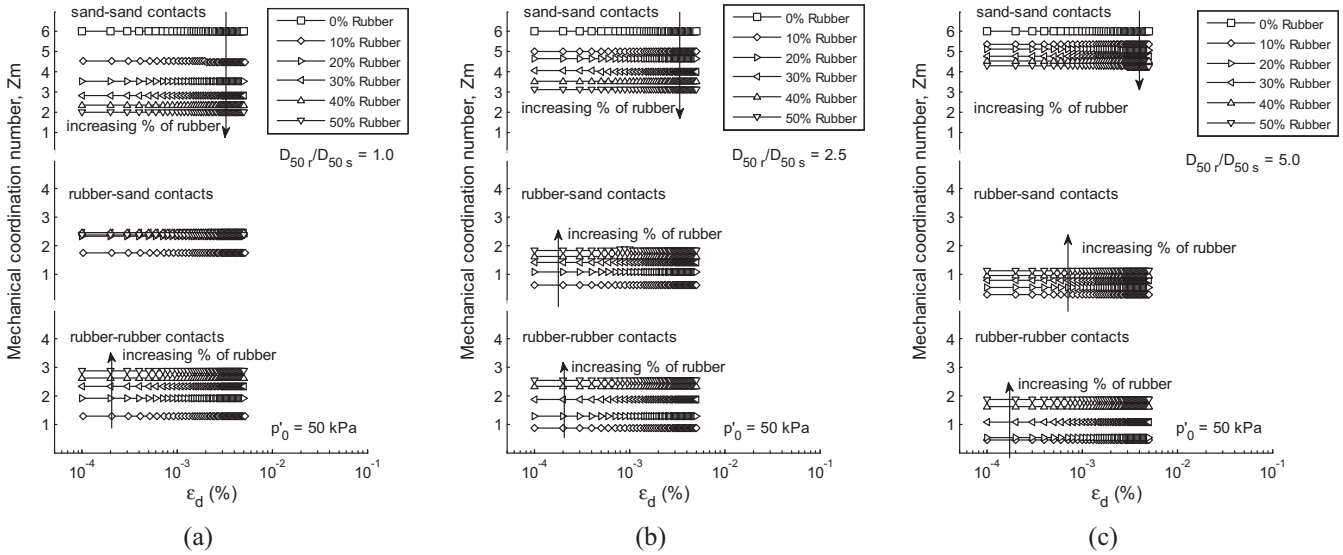

Fig. 6. Mechanical coordination number against shear strain by type of contact for (a) D_{50R}/D_{50S} of 1.0, (b) D_{50R}/D_{50S} of 2.5 and (c) D_{50R}/D_{50S} of 5.0.

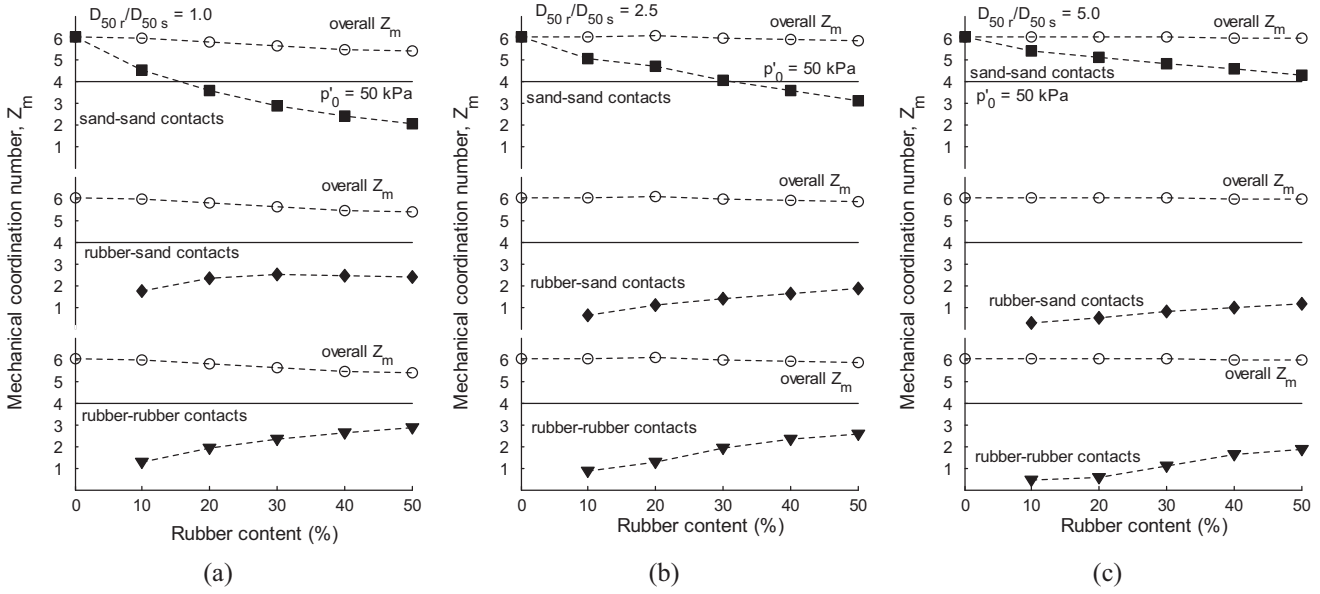

Fig. 7. Overall mechanical coordination number at G_{max} and mechanical coordination number by type of contact for (a) D_{50R}/D_{50S} of 1.0, (b) D_{50R}/D_{50S} of 2.5 and (c) D_{50R}/D_{50S} of 5.0.

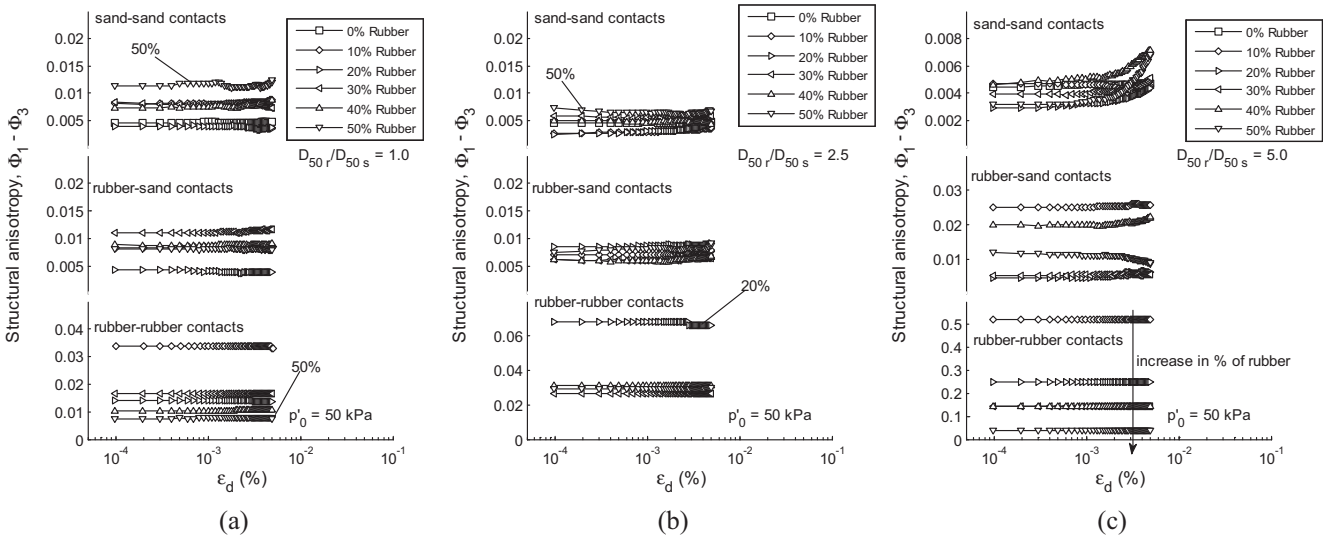

Fig. 8. Structural anisotropy against shear strain by type of contact for (a) D_{50R}/D_{50S} of 1.0, (b) D_{50R}/D_{50S} of 2.5 and (c) D_{50R}/D_{50S} of 5.0.

(Φ_1-Φ_3) in the order of 10^{-3}. However, interesting patterns are noticeable after an examination of (Φ_1-Φ_3) for each type of contact. Mixtures with $D_{50R}/D_{50S} = 1$ show values of (Φ_1-Φ_3) close to the overall for sand-sand contacts up to a rubber content of 20%, from which (Φ_1-Φ_3) increases with rubber content while the overall deviatoric anisotropy decreases. The slight increase of structural anisotropy for sand-sand contacts is due to the appearance of more rubber-involved contacts that lowers the structural anisotropy for rubber-rubber contacts. For a ratio of $D_{50R}/D_{50S} = 5.0$, (Φ_1-Φ_3) for sand-sand contacts virtually overlaps with the overall (Φ_1-Φ_3) and shows an even more isotropic structure as noticed for the case of rubber content of 40% indicating the presence of rubber particles embedded in a sand skeleton.

The general trend for rubber-rubber contacts is to attain a more isotropic contact network as rubber content increases, regardless of the D_{50R}/D_{50S} ratio. More rubber-rubber contacts increase the chance of these contacts to be aligned in all directions which will be maintained due to the high inter-particle friction. The effect of rubber content on rubber-rubber contacts (Φ_1-Φ_3) is more significant as D_{50R}/D_{50S} increases.

No clear trend is appreciated for rubber-sand contacts for all D_{50R}/D_{50S} ratios. It should be noted that in some cases values of rubber-sand contacts (Φ_1-Φ_3) being close to the overall (Φ_1-Φ_3) do not necessarily indicate an isotropic rubber-sand network due to the low value of $Z^{r\text{-}s}$. It only indicates rubber-sand contacts isotropically distributed but in isolated locations within the system. High values of structural anisotropy are linked to the formation of lines of rubber-rubber contacts leaving rubber-sand contacts surrounding these as a second part of the solid skeleton. While values of structural anisotropy close to the overall indices the presence of floating rubber particles that are surrounded in all directions by sand particles.

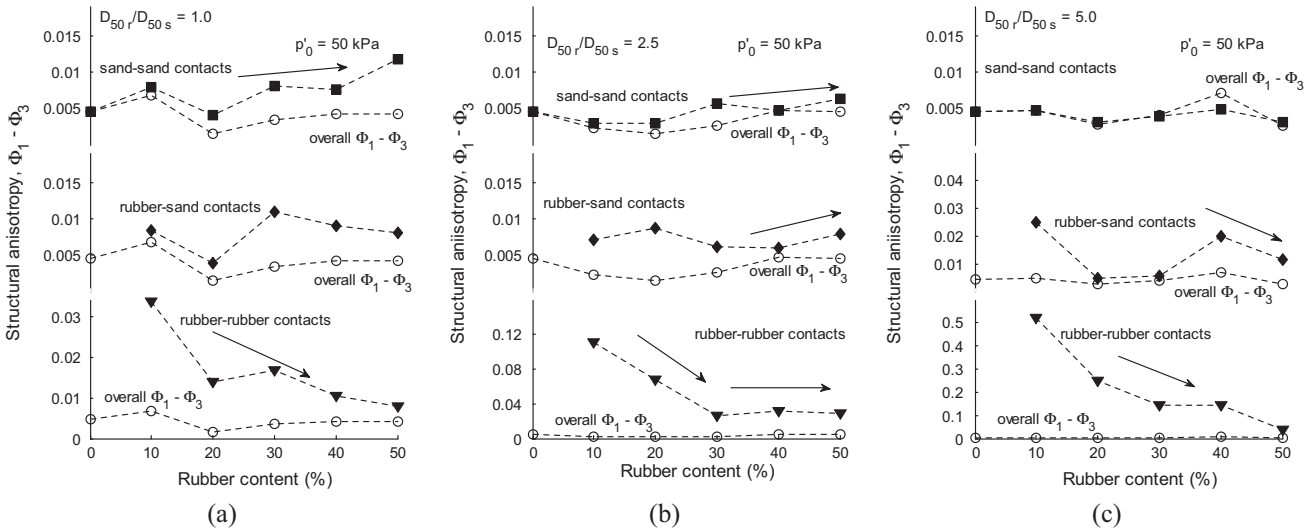

Fig. 9. Overall structural anisotropy at G_{max} and structural anisotropy by type of contact for (a) D_{50R}/D_{50S} of 1.0, (b) D_{50R}/D_{50S} of 2.5 and (c) D_{50R}/D_{50S} of 5.0.

4.2.3. Normal contact force anisotropy

Stresses in a granular material are strongly related to different sources of anisotropy, which includes geometrical anisotropy, as discussed above, and the normal contact force anisotropy (a_n), as Rothenburg and Bathurst [48] showed analytically. The sources of different stress levels observed in Fig. 4 and differences in G_{max} as rubber content and D_{50R}/D_{50S} increase are expected to be related to a_n. The average normal contact force tensor is expressed in Eq. (2) (where Φ'_{ij} is the deviatoric part of Φ_{ij}) with its probability distribution given by Eq. (3) and $a^n_{ij} = (15/2)F^n_{ij}/\bar{f}^0$ [17,48]. $\bar{f}^0 = F^n_{ii}$ is the average normal contact force calculated considering the entire space Ω (enclosed in the periodic cell), which can be deferred from the mean normal contact force averaged over all contacts. a_n is related to the second invariant of a^n_{ij} as $a_n = \sqrt{(3/2)a^n_{ij}a^n_{ij}}$.

$$F^n_{ij} = \frac{1}{4\pi}\int_{\Omega}\overline{f_n}(\Omega)n_i n_j d\Omega = \frac{1}{N_c}\sum_{1}^{N_c}\frac{f_n n_i n_j}{1+(15/2)\Phi'_{ij}n_k n_l} \tag{2}$$

$$\overline{f_n}(\Omega) = \bar{f}^0[1+a^n_{ij}] \tag{3}$$

An overall F^n_{ij} considering all the contacts, plus a F^n_{ij} focusing on each type of contact, were obtained. Similarly, the overall a_n and a_n for each type of contact were calculated. Fig. 10(a)–(c) include a_n against ε_d for each type of contact and D_{50R}/D_{50S} respectively. An initial observation is that a_n for sand-sand and rubber-sand contacts does not remain constant during the shearing stage and starts to increase exponentially from around ε_d = 1e−3, with the exception of sand-sand contacts for a D_{50R}/D_{50S} equal to 1.0 that shows a gentle decrease in a_n. Sand-sand contacts present interesting trends in a_n that depend on the strain level. For D_{50R}/D_{50S} = 1 and 2.5, a_n increases with rubber content at very small stains; however, when ε_1 > 1e−3, a_n is found to decrease as rubber content increases. An increase in a_n with rubber content is noticed for all range of ε_1 when D_{50R}/D_{50S} = 5.0. Rubber-sand contacts do not present a clear trend. Only at ε_1 > 1e−3 does a_n seem to decrease as rubber content increases for the case of D_{50R}/D_{50S} = 1.0, while the opposite trend is observed for D_{50R}/D_{50S} = 5.0. The highest rate of increase of a_n is observed for mixtures having D_{50R}/D_{50S} = 2.5, while the slowest rate of increase that is affected simultaneously by rubber content corresponds to the mixture with D_{50R}/D_{50S} = 1.0. Regardless of rubber content and D_{50R}/D_{50S}, sand-sand and rubber-sand contacts achieve similar values of a_n in the same order of magnitude. Rubber-rubber contacts show higher values of a_n as D_{50R}/D_{50S} increases. Additionally, a_n decreases as rubber content increases in mixtures with D_{50R}/D_{50S} of 2.5 and 5.0. For rubber-rubber contacts, there is no change in the structural anisotropy as shown in Fig. 7 due to their lack of rearrangement (high inter-particle friction). Any increase in the force carried by rubber-rubber contacts will be transmitted by a steady contact structure keeping the normal contact force anisotropy steady. This indicates that these contacts tend to orientate orthogonal to the loading direction that together with their inability to re-accommodate would hinder their chance of altering the manner in which these contacts transmit forces.

With a_n being the main contributor to the overall strength of the system, the more pronounced decays in deviatoric strength for mixtures with D_{50R}/D_{50S} = 1.0 and D_{50R}/D_{50S} = 2.5 as strain level increases are related to decays in a_n for sand-sand contacts during the same stage of deformation, and an increase in a_n for rubber-sand contacts, which in turn affects the amount of stress that the system can transmit. For the case of D_{50R}/D_{50S} = 5.0, as rubber content increases, a_n for sand-sand contacts always increases regardless of the axial deformation, restricting both rubber-sand and rubber-rubber contacts from taking part in the stress transmission. This prevented q to be reduced as rubber content increased in the mixtures with D_{50R}/D_{50S} = 5.0.

From Fig. 11 it is appreciated how the overall a_n increases as rubber content increases, especially for the cases of D_{50R}/D_{50S} = 2.5 and D_{50R}/D_{50S} = 5.0. A more gentle increase is still noticeable for D_{50R}/D_{50S} = 1. Sand-sand contacts from a D_{50R}/D_{50S} of 1 show an increase in a_n with rubber content; in D_{50R}/D_{50S} = 2.5, an increase of a_n is seen up to a rubber content of 30%, when a_n begins to decrease with the increase in rubber content to values below the overall. Values of a_n appear close to the overall for the case of D_{50R}/D_{50S} = 5.0. Rubber–sand contacts for mixtures having D_{50R}/D_{50S} = 1 present an interesting peak in a_n when the rubber content is 30%, which coincides with values of $Z^{r\text{-}s}$ lower than 4; from 30% onwards, a_n decreases with rubber content to values below the overall a_n. Samples with D_{50R}/D_{50S} = 2.5 and D_{50R}/D_{50S} = 5.0 show higher values of a_n than the overall for all contents of rubber. Rubber-rubber contacts for the case of D_{50R}/D_{50S} = 1 decrease in a_n as rubber content increases up to 30%, marking a minimum in a_n for rubber-rubber contacts that happens simultaneously with the transition from stable to unstable sand-sand contact network. In mixtures with D_{50R}/D_{50S} = 2.5, no clear trend of a_n is observed.

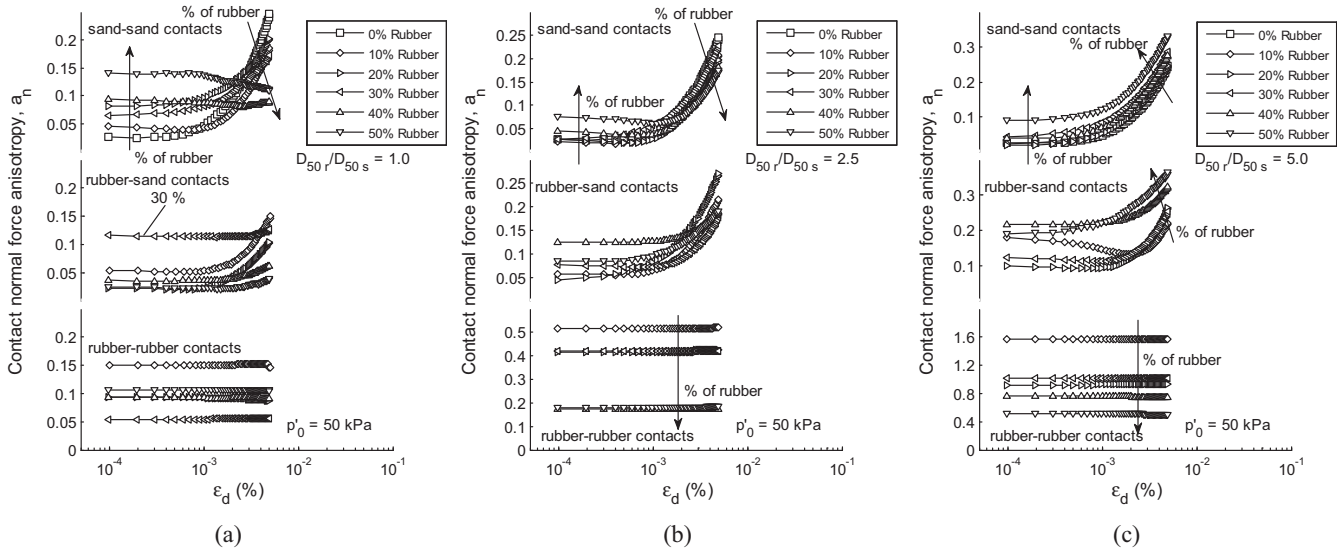

Fig. 10. Normal contact force anisotropy against shear strain by type of contact for (a) D_{50R}/D_{50S} of 1.0, (b) D_{50R}/D_{50S} of 2.5 and (c) D_{50R}/D_{50S} of 5.0.

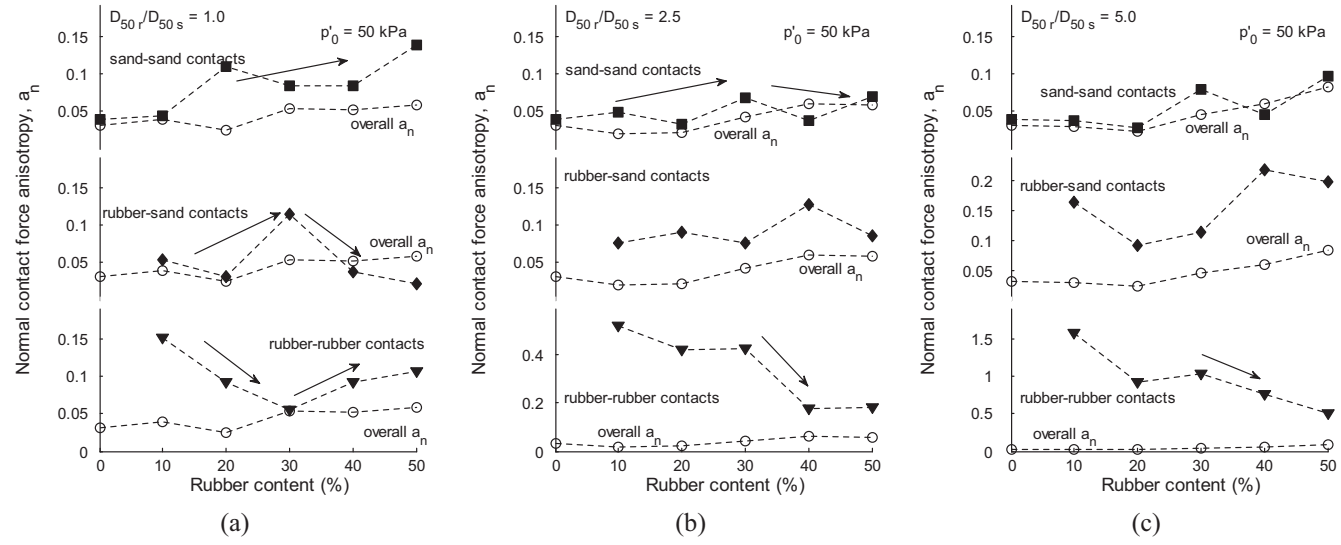

Fig. 11. Overall normal contact force anisotropy at G_{max} and normal contact force anisotropy by type of contact for (a) D_{50R}/D_{50S} of 1.0, (b) D_{50R}/D_{50S} of 2.5 and (c) D_{50R}/D_{50S} of 5.0.

A clear decrease in a_n with rubber content is observed in samples with D_{50R}/D_{50S} = 5.0, however, a_n remains almost two orders of magnitude larger than the overall a_n. Rubber-rubber contacts present more distanced values of a_n from the overall as D_{50R}/D_{50S} increases. The inspection of the micro-parameters at the very small strains reveals that there is an interaction between the packing density at the contact scale and the different sources of anisotropy as rubber content and particle size increases, which finally affected markedly the mixtures stress-strain response and stiffness (G_{max}).

The contractive response observed in Fig. 3(b) can be associated with the particle scale response of both samples. As commented by Yimsiri and Soga [66] the initial stress response of a granular system is dependent on the initial contact anisotropy and normal contact force anisotropy. When normal contact forces are oriented in the vertical direction more dilative response is expected, for the case of the pure sand the normal contact force anisotropy is the lowest, leading to an initial contraction. While for the test M50-1:1-50 the initial contact normal anisotropy is the highest, it starts decreasing when a strain level of 1e−3 is reached, coinciding with a decrease in p'.

The value of G_{max} shown in Fig. 4(b) was calculated before the elastic threshold was reached [41]. An indicator of this is that Z_m and (Φ_1-Φ_3) remained constant in the range of ε_1 = 1e−4 to ε_1 = 1e−3, denoting that there was no re-arranging of particles or complete detachment of contacts taking place, which could lead to plastic deformations within the sample [38]. Differences observed in G_{max} for different rubber content and D_{50R}/D_{50S} can be explained by the micro-mechanical response from the simulated samples in the range of ε_1 = 1e−4 to ε_1 = 1e−3. G would be micro-mechanically dependent on: how the overall stability of the system is shared among the different types of contacts, that allows the transmission of stresses within the boundaries of the system and in what direction do the forces act on those contacts being concentrated.

4.2.4. Contact rose diagrams

The influence of the number of contacts, the structural anisotropy and the normal contact force anisotropy on G_{max} is illustrated by rose diagrams of each type of contact for rubber contents of 10%, 30% and 50%, in all size ratios, in Figs. 12–14. The radial length of each bin gives the number of contacts present in the angles bounded by the bin. The colour is proportional to the average normal contact force that is oriented in each bin normalized by the total average normal force within the entire sample.

Considering first the case of a D_{50R}/D_{50S} of 1.0 (Fig. 12), with a rubber content of 10%, sand-sand and rubber-sand contacts are seen to carry a similar amount of average normal contact force in each bin, leading to a higher transmission of forces through sand-sand contacts due to the larger number of sand-sand contacts available. Very few rubber-rubber contacts are carrying less than average normal contact force. At a rubber content of 10%, the system is clearly sand dominated. For rubber content of 30%, the stiffness and the strength of the system are controlled by rubber particles, with rubber-sand contacts being the major type of contact. More contacts were oriented vertically, parallel to the direction of loading and having slightly: greater average magnitude of normal force. Rubber-rubber contacts become important at this point due to the similar orientations of the larger number of these contacts available. With sand-sand contacts the fewest in number at rubber content of 50%, contacts that involve rubber particles are the majority, which at the same time are oriented isotropically, allowing the transmission of forces in all directions resulting in an overall strength of the system being controlled by rubber particles.

Comparable results are observed from the rose diagrams relating rubber particles with D_{50R}/D_{50S} = 2.5 included in Fig. 13. While the number of sand-sand contacts reduces as rubber content increases, both rubber-sand and rubber-rubber contacts increase in number. Rubber-rubber contacts are seen to carry the strong normal contact force at all rubber contents. As the stiffer sand-sand contacts carry weak normal contact force, the strength of the system reduces; As previously noted, in mixtures with D_{50R}/D_{50S} = 5.0, the contacts present in the system are dominated by sand-sand contacts that carry the least average normal contact force while the average normal contact force transmitted through the small number of rubber-rubber contacts is the highest. Experimental observations of increase in stiffness with content of large rubber particles by Kim and Santamarina [26] can be explained from the rose diagrams. Although sand-sand contacts have the

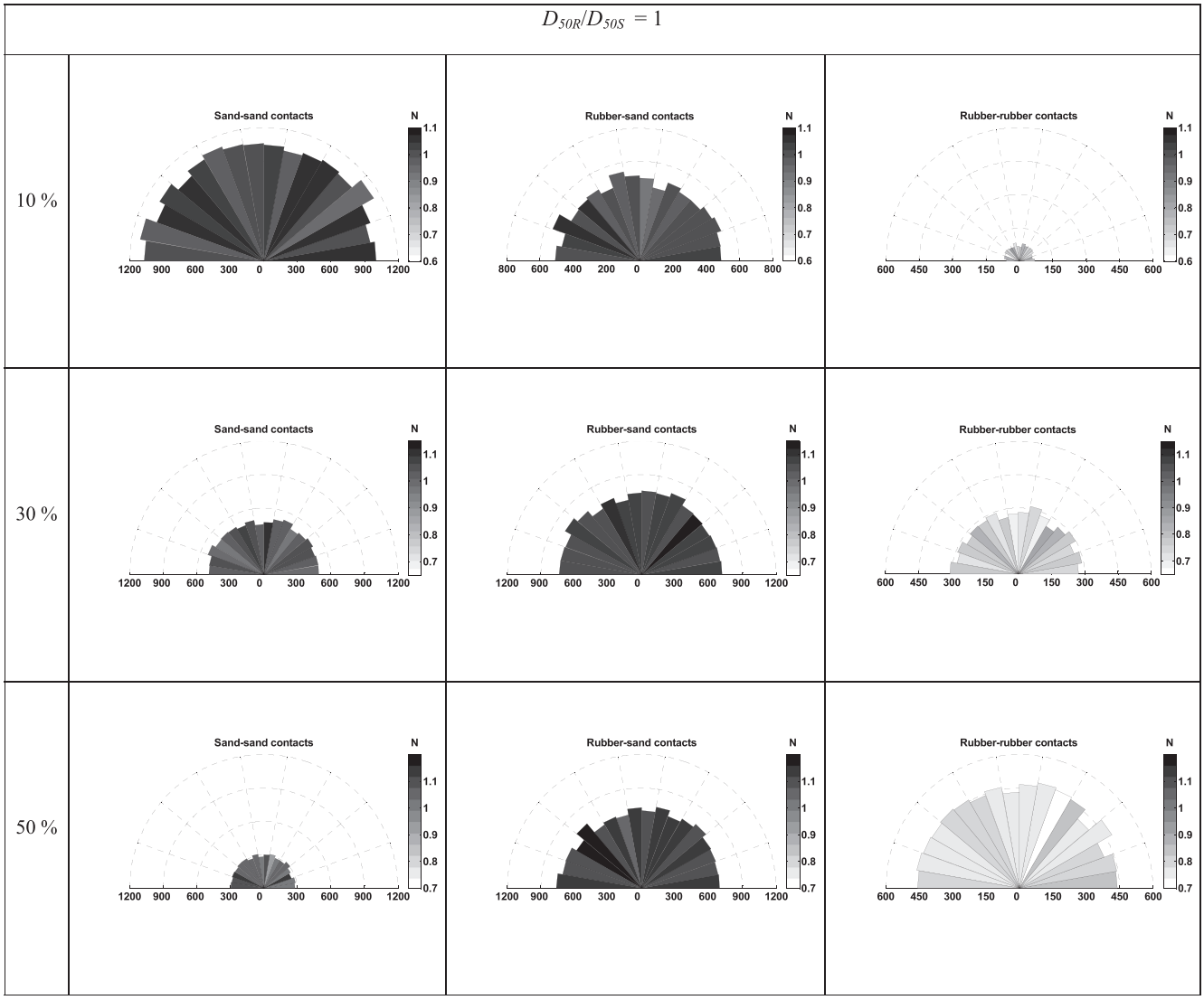

Fig. 12. Rose diagrams at G_{max} for rubber contents of 10%, 30% and 50% with D_{50R}/D_{50S} = 1.0 shared from p'_0 = 50 kPa.

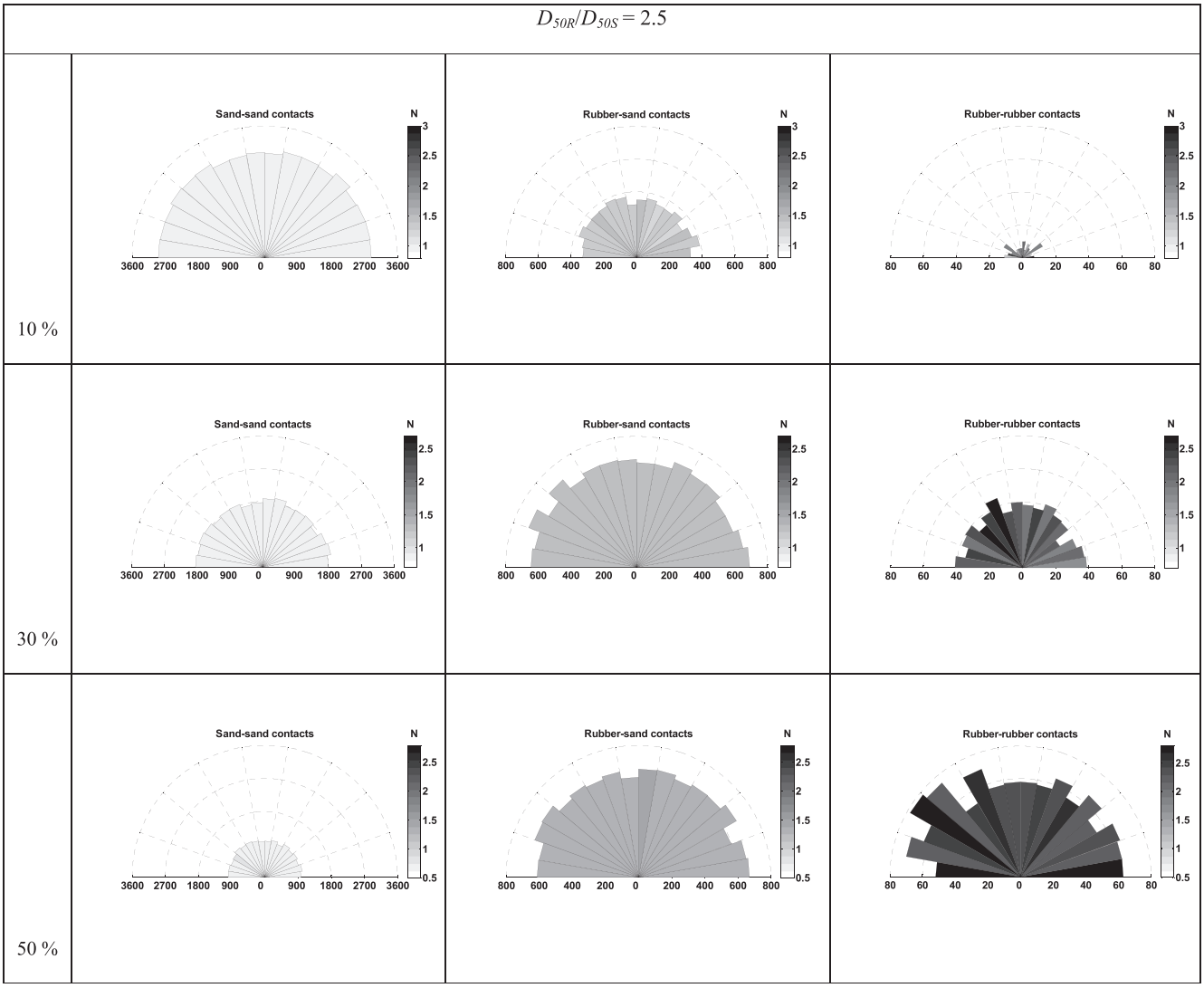

Fig. 13. Rose diagrams at G_{max} for rubber contents of 10%, 30% and 50% with $D_{50R}/D_{50S} = 2.5$ shared from $p'_0 = 50$ kPa.

lowest average normal contact force, due to the large number of this contacts, the total force being carried by sand-sand contacts is greater than rubber-sand or rubber-rubber contacts, making sand-sand contacts control the overall strength of the system when $D_{50R}/D_{50S} = 5.0$ as observed in Fig. 14. Rubber-rubber contacts, on the other hand, are very weak due to their small number and random distribution. No clear bias for the average normal force in orientation is perceived from the rose diagrams. However, where a weak normal contact force is seen for a certain type of contact at a distinct bin, a strong normal contact force from a different type of contact will compensate at the exact direction, contributing to the overall low values of a_n.

4.2.5. Contribution to deviatoric stress

Fig. 15 shows, for all D_{50R}/D_{50S} considered, the cumulative contribution to the deviatoric stress and from all and each type of contact at the end of shearing as a function of the normal contact force normalized by the average normal contact force ($f_n/\langle f_n \rangle$) following Radjai et al. [46]. The overall q at the end of shearing is given by the final point of each curve corresponding to all contacts. An initial observation is that greater contact forces appear as rubber content and D_{50R}/D_{50S} increase.

In mixtures with $D_{50R}/D_{50S} = 1.0$, for a rubber content of 50%, the q available is due to the contribution of either rubber-sand or rubber-rubber contacts. At the same percentage of rubber but considering $D_{50R}/D_{50S} = 2.5$, rubber-sand contacts contribute the most to a positive q while rubber-rubber contacts with $f_n/\langle f_n \rangle > 1.0$ are seen contributing negatively to the overall q. Mixtures with $D_{50R}/D_{50S} = 5.0$ at a rubber content of 50% reveal that almost all the contribution to the overall q is made by sand-sand contacts at $f_n/\langle f_n \rangle$ less than 10. Any positive contribution from rubber-sand contacts is erased by rubber-rubber contacts that are either contributing negatively to q or tended to reduce the overall q.

4.2.6. Contact force networks

For a thorough illustration of the effect of rubber content on the contact force network, Fig. 16 presents, for all D_{50R}/D_{50S} considered the contact force network at the end of shearing at a rubber content of 50%. Different contact networks are shown corresponding to: all contacts, sand-sand, rubber-sand and the rubber-rubber contacts. The width and colour of the lines are proportional to the contact force magnitude. The contact force network in mixtures with $D_{50R}/D_{50S} = 1.0$ is clearly dominated by rubber-sand or rubber-rubber contacts that are found able to transmit stresses

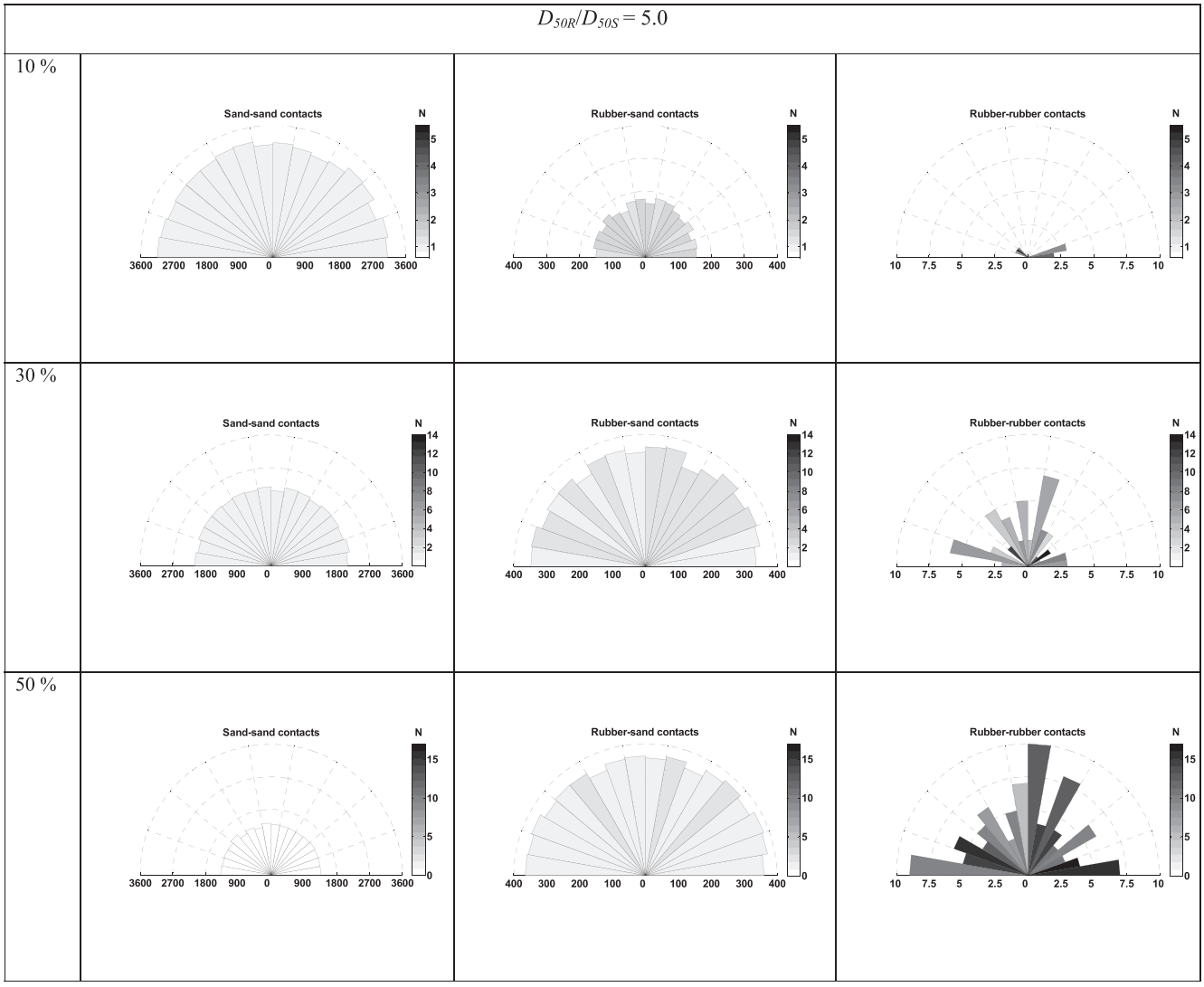

Fig. 14. Rose diagrams at G_{max} for rubber contents of 10%, 30% and 50% with D_{50R}/D_{50S} = 5.0 shared from p'_0 = 50 kPa.

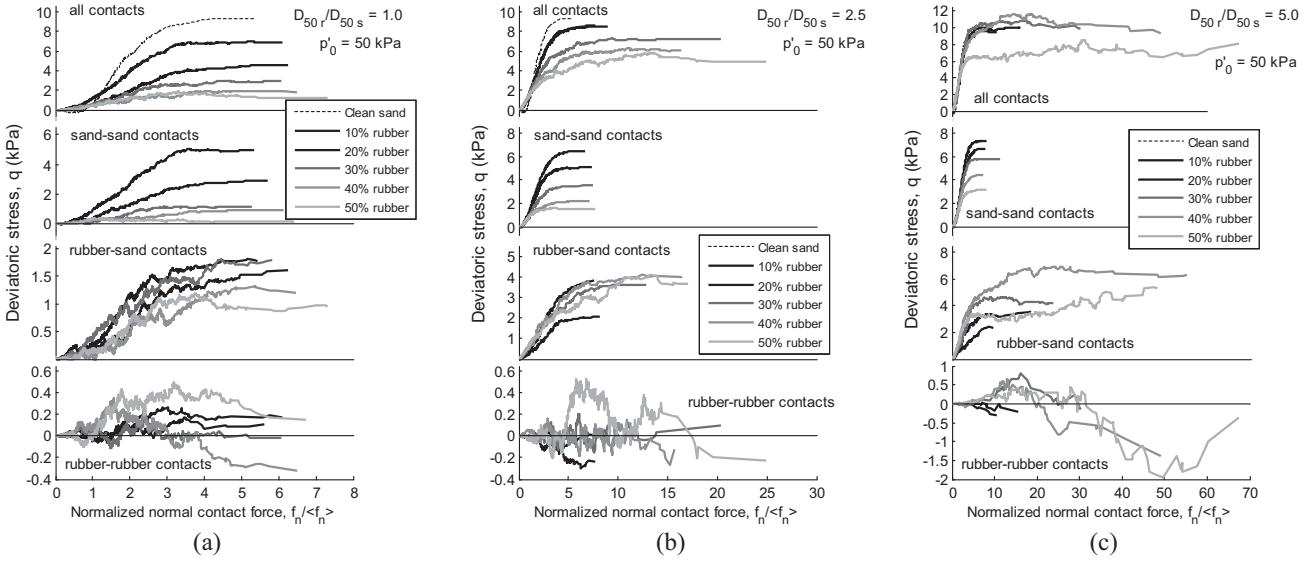

Fig. 15. Contribution to the deviatoric stress at the end of test from all contacts and each type of contacts at different percentages of rubber and rubber sizes of (a) D_{50R}/D_{50S} = 1.0, (b) D_{50R}/D_{50S} = 2.5 and (c) D_{50R}/D_{50S} = 5.0.

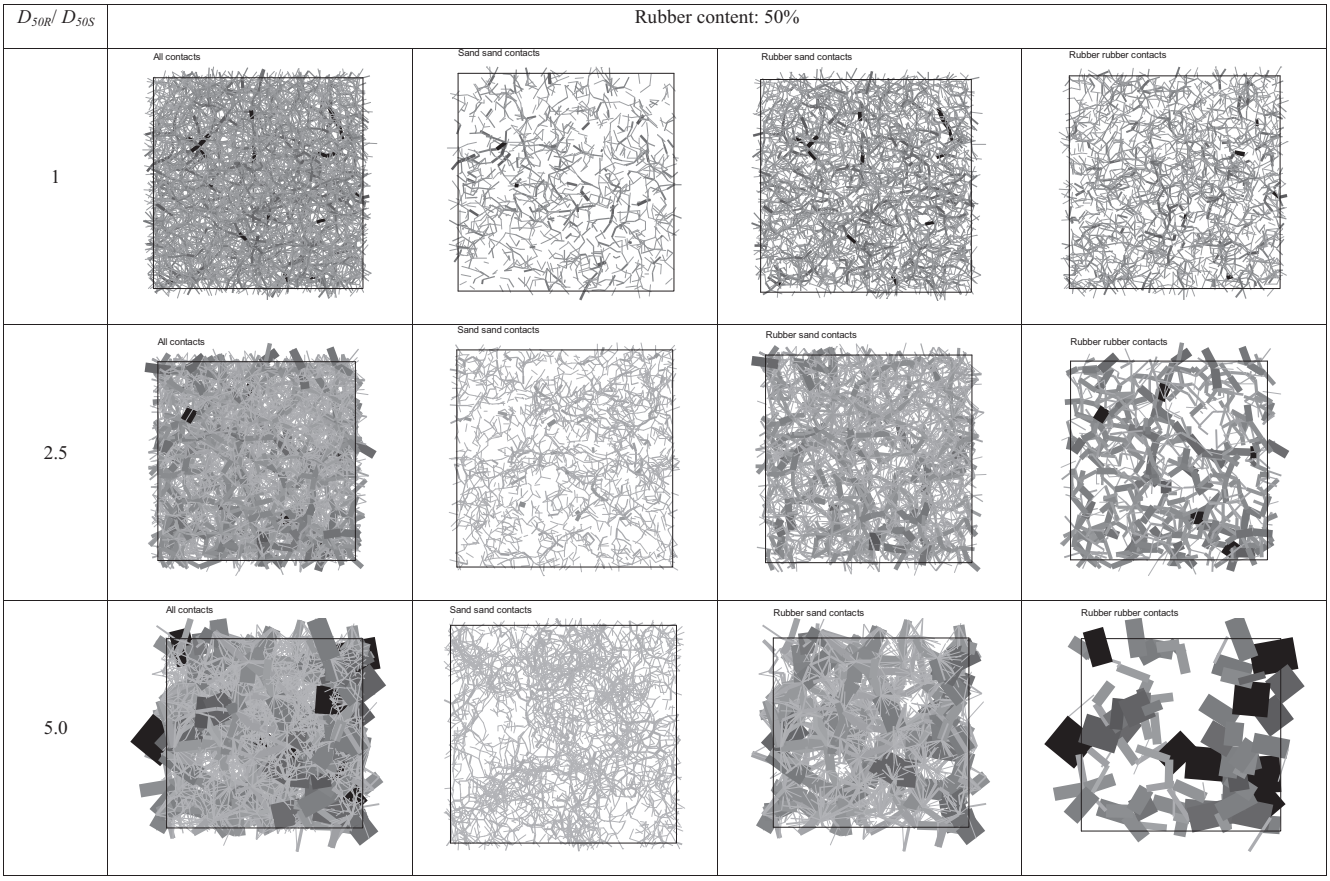

Fig. 16. Contact force network at the end of test for all rubber sizes at a rubber content of 50%. Samples shown are sheared from p'_0 = 50 kPa.

among the cell boundaries. Sand-sand contacts, on the other hand, are seen disperse and isolated, unable to form a stable contact network. A similar case is observed for D_{50R}/D_{50S} = 2.5, however, the contact network formed by rubber-sand contacts is the one seemingly more capable of transmitting stresses within the sample. Sand-sand contacts with D_{50R}/D_{50S} = 5.0 are seen to form a stable contact network in between the rubber particles; while fewer in number, rubber-sand contacts appear to form a contact network also capable of stress transmission within the cell boundaries. The negative contribution to q observed above from rubber-rubber contacts can be visualized in the rubber-rubber contact network that is not seen able to transmit forces within the boundaries of the cell, plus most contacts remain aligned orthogonal to the direction of loading.

It should be noted that the macro and micro-mechanical trends observed in the stress-strain response and stiffnesses of samples were consistent for all p'_0 considered. The discussion of the micro-mechanical response addressed above is valid for the stress levels considered in this study. The similar trends found in the laboratory and simulation results suggest that the sensitivity of the mixture behaviour to size ratio is independent of the absolute size of particles.

5. Conclusions

DEM simulations of sand-rubber mixtures tested under triaxial monotonic compression at constant volume conditions were discussed, focusing on different levels of deformation ranging from very small to small strains. A systematic study on the behaviour of sand-rubber mixtures was subsequently conducted, using rubber contents that ranged from 10% to 50% by mixture weight and D_{50R}/D_{50S} ratios of 1.0, 2.5 and 5.0. The macro-mechanical response and the prevailed micro-mechanisms experienced by those mixtures were explored.

The macro-response of the simulated mixtures showed a decrease in the elastic shear modulus and strength with increasing rubber content for D_{50R}/D_{50S} ratios of 1.0 and 2.5, while the opposite trend was found for D_{50R}/D_{50S} ratios of 5. This was in quantitative and qualitative agreement with previous published laboratory test results.

The micro-mechanics developed in the range of very small strains provide an explanation to the effect of rubber content and particle size on G_{max} ($G = (2/3)q/\varepsilon_q$). A capable contact network having an adequate number of contacts, oriented isotropically within the sample, was seen to be leading the force transmission in the system and therefore having an important effect on G_{max}.

More evident changes in q as rubber content increased for different stages of deformation are linked to the different trends observed in a_n during the shearing stage. At the end of the test for mixtures involving D_{50R}/D_{50S} ratios of 1.0 and 2.5, contact networks formed by sand-sand and rubber-sand contacts transmit normal forces in a less biased fashion to the loading direction that ends up influencing q. In contrast, mixtures involving large rubber particles a_n for sand-sand and rubber-sand particles were always seen to increase, which resulted in no significant effect on q.

Clear size effects of rubber particles on the mechanical behaviour of the mixtures were observed when considering the contribution to q by each type of contact. Rubber particles that have the same size with sand particles are able to contribute positively to q by either rubber-sand or rubber-rubber contacts. As the size of rubber particles increased, it was mainly the rubber-sand contacts

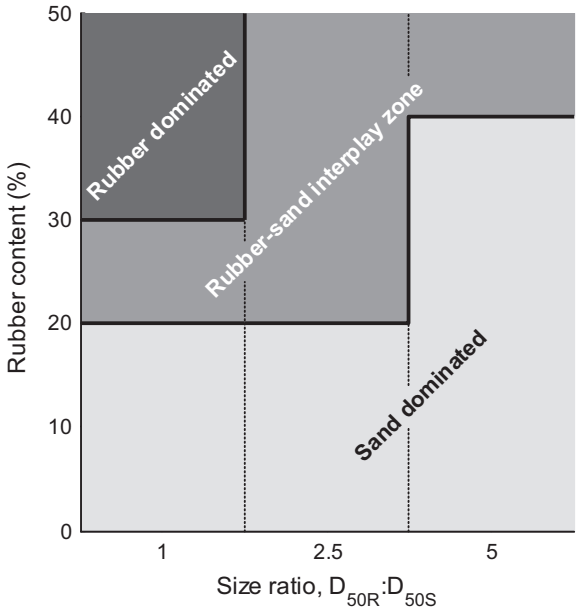

Fig. 17. Phase diagram for sand-rubber mixtures.

that contribute positively to q; rubber-rubber contacts, on the other hand, tend to decrease the overall q ($D_{50R}/D_{50S} = 2.5$), and at larger rubber sizes clearly contribute negatively to q ($D_{50R}/D_{50S} = 5.0$).

Based on the macro and particle scale results, Fig. 17 shows a diagram of the three possible phases for sand-rubber mixtures, taking into account both size ratio and rubber contents up to 50%. A sand dominated response is observed for size ratios of 1.0 and 2.5 up to rubber contents of 20%. A rubber dominated response is only perceived for a size ratio of 1.0 and from rubber contents greater than 30%. Larger rubber particles would require a greater rubber content to become participant in the overall strength of the sample, for a size ratio of 5.0 this is only seen happening for rubber contents greater than 40%.

The size and percentage of rubber particles should be selected depending on the purpose of use for the mixtures. For the range of strains considered in this study, mixtures with $D_{50R}/D_{50S} = 1.0$ showed an increase in void ratio with rubber content which would be helpful to improve drainage conditions. A reduction in deviatoric stress was observed for samples having either D_{50R}/D_{50S} of 1.0 or 2.5 indicating their usability for stress and settlement reduction. Mixtures with $D_{50R}/D_{50S} = 5.0$ gave the best mechanical behaviour, mostly because of these samples being sand-dominated. For all rubber contents, the strength of the samples remained virtually the same when compared with the pure sand response. Besides, only for $D_{50R}/D_{50S} = 5.0$ G_{max} was seen to increase with rubber content. The micro-mechanics explored, show that although sand dominated, these samples would still be benefited with the advantageous rubber particles properties such as low unit weight and high damping as rubber particles were seen to participate actively in the contact force network, especially for rubber-sand contacts.

Acknowledgments

The authors would like to acknowledge the anonymous reviewers for their constructive comments that helped us to improve the quality of the manuscript. This study was supported by The University of Hong Kong SPACE research fund. This research was conducted using the HKU Information Technology Services research computing facilities that are supported in part by the Hong Kong UGC Special Equipment Grant (SEG HKU09). The third author would like to acknowledge a grant from the Faculty of Engineering UNSW (FRG PS38513) for supporting his trips to Hong Kong for collaboration.

References

[1] Anastasiadis A, Senetakis K, Pitilakis K. Small-strain shear modulus and damping ratio of sand-rubber and gravel-rubber mixtures. Geotech Geol Eng 2012;30(2):363–82.
[2] Barreto D, O'Sullivan C. The influence of inter-particle friction and the intermediate stress ratio on soil response under generalised stress conditions. Granular Matter 2012;14(2):505–21.
[3] Bagi K. Stress and strain in granular assemblies. Mech Mater 1996;22(3):165–77.
[4] Beatty JR. Physical properties of rubber compounds. In: Clark SK, editor. Mechanics of Pneumatic Tires. Washington, DC: National Highway Traffic Administration, U.S. Department of Transportation; 1991.
[5] Bernal A, Salgado R, Swan Jr RH, Lovell CW. Interaction between tire shreds, rubber-sand and geosynthetics. Geosynth Int 1997;4(6):623–43.
[6] Bosscher PJ, Edil TB, Kuraoka S. Design of highway embankments using tire chips. J Geotech Geoenviron Eng ASCE 1997;123(4):295–304.
[7] Bolton MD. The strength and dilatancy of sands. Géotechnique 1986;36(1):65–78.
[8] Cundall PA, Strack ODL. A discrete element model for granular assemblies. Géotechnique 1979;29(1):47–65.
[9] daCruz F, Emam S, Prochnow M, Roux JN, Chevoir F. Rheophysics of dense granular materials: discrete simulation of plane shear flows. Phys Rev E 2005;72:021309.
[10] Edeskar T. Use of tyre shreds in civil engineering applications—Technical and environmental properties Ph.D. Dissertation. Sweden: Lulea University of Technology, Department of Civil and Environmental Engineering, Division of Mining and Geotechnical Engineering; 2006.
[11] Edil TB. A review of mechanical and chemical properties of shredded tires and soil mixtures. In: Aydilek AH, Wartman J, editors. Recycled materials in geotechnics, geo-technical special publication, No. 127. ASCE; 2004. p. 1–21.
[12] Edincliler A. Using waste tire-soil mixtures for embankment construction. In: Hazarika, Yasuhara, editors. Proceedings of the international workshop on scrap tire derived geomaterials-opportunities and challenges, Yokosuka, Japan. p. 319–28.
[13] Edincliler A, Ayhan V. Influence of tyre fiber inclusions on shear strength of sand. Geosynth Int 2010;17(4):183–92.
[14] Edincliler A, Cagatay A. Weak subgrade improvement with rubber fibre inclusions. Geosynth Int 2013;20(1):39–46.
[15] Evans TM, Valdes JR. The microstructure of particulate mixtures in one-dimensional compression: numerical studies. Granular Matter 2011;13(5):657–69.
[16] Gu X, Huang M, Qian J. DEM investigation on the evolution of microstructure in granular soils under shearing. Granular Matter 2014;16(1):91–106.
[17] Guo N, Zhao J. The signature of shear-induced anisotropy in granular media. Comput Geotech 2013;47:1–15.
[18] Hazarika H, Kohama E, Sugano T. Underwater shake table tests on waterfront structures protected with tire chips cushion. J Geotech Geoenviron Eng ASCE 2008;134(12):1706–19.
[19] Hecke MV. Jamming of soft particles: geometry, mechanics, scaling and isostaticity. J Phys: Condense Matter 2010;22(3):033101.
[20] Huang X, O'Sullivan C, Hanley KJ, Kwok CY. Discrete-element method analysis of the state parameter. Géotechnique 2014;64(12):954–65.
[21] Huang X, Hanley KJ, O'Sullivan C, Kwok CY. Effect of sample size on the response of DEM samples with a realistic grading. Particuology 2014;15:107–15.
[22] Huang X. Exploring critical-state behaviour using DEM Ph.D. Thesis. The University of Hong Kong – Imperial College London; 2014.
[23] Humphrey D, Sandford T. Tire chips as lightweight subgrade fill and retaining wall backfill. In: Proceedings of recycling ahead, October 19–22, Denver, USA.
[24] Humphrey D, Cosgrove T, Whetten NL, Herbert R. Tire chips reduce lateral earth pressure against the walls of a rigid frame bridge. In: Seminar on rehabilitation and upgrades in civil and environmental engineering. ASCE; 1997.
[25] Kaneda K, Hazarika H, Yamazaki H. The numerical simulation of earth pressure reduction using tire chips in backfill. In: Hazarika, Yasuhara, editors. Proceedings of the international workshop on scrap tire derived geomaterials—opportunities and challenges, Yokosuka, Japan. p. 245–51.
[26] Kim HK, Santamarina JC. Sand–rubber mixtures (large rubber chips). Can Geotech J 2008;45(10):1457–66.
[27] Lee JH, Salgado R, Bernal A, LovellC W. Shredded tires and rubber-sand as lightweight backfill. J Geotech Geoenviron Eng ASCE 1999;125(2):132–41.
[28] Lee JS, Dodds J, Santamarina JC. Behavior of rigid-soft particle mixtures. J Mater Civ Eng 2007;19(2):179–84.
[29] Lee C, Truong QH, Lee W, Lee JS. Characteristics of rubber-sand particle mixtures according to size ratio. J Mater Civ Eng 2010;22(4):323–31.
[30] Lee C, Shin H, Lee J. Behaviour of sand-rubber particle mixture: experimental observations and numerical simulations. Int J Numer Anal Meth Geomech 2014;38(16):1651–63.

[31] Lopera Perez JC, Kwok CY, O'Sullivan C, Huang X, Hanley KJ. Assessing the quasi-steady conditions for shearing in granular media within the critical state soil mechanics framework. Soils Found 2016;56(1):152–9.
[32] Mashiri MS, Vinod JS, Sheikh MN, Tsang H. Shear strength and dilatancy behaviour of sand-tyre chip mixtures. Soils Found 2015;55(3):517–28.
[33] Mavronicola E, Komodromos P, Charmpis D. Numerical investigation of potential usage of rubber-soil mixtures as a distributed seismic isolation approach. In: Adam JM, Pallare FJ, Bru R, Romero ML, editors. Proceedings of the tenth international conference on computational structures technology. Stirlingshire (UK): Civil-Comp Press; 2010 [Paper 168].
[34] MiDi GDR. On dense granular flows. Euro Phys J, E 2004;14(4):341–65.
[35] Mindlin RD, Deresiewicz H. Elastic spheres in contact under varying oblique forces. J Appl Mech 1953;20:327–44.
[36] Minh NH, Cheng YP. A DEM investigation of the effect of particle-size distribution on one-dimensional compression. Géotechnique 2013;63(1):44–53.
[37] Narejo DB, Shettima M. Use of recycled automobile tires to design landfill components. Geosynth Int 1995;2(3):619–25.
[38] O'Donovan J, O'Sullivan C, Marketos G. Two-dimensional discrete element modelling of bender element tests on an idealised granular material. Granular Matter 2013;14(6):733–47.
[39] O'Sullivan C, Bray J. Selecting a suitable time step for discrete element simulations that use the central difference time integration scheme. Eng Comput 2004;21(2/3/4):278–303.
[40] Özkul ZH, Baykal G. Shear behavior of compacted rubber fiber-clay composite in drained and undrained loading. J Geotech Geoenviron Eng 2007;133(7):767–81.
[41] Oztoprak S, Bolton MD. Stiffness of sands through a laboratory database. Géotechnique 2013;63(1):54–70.
[42] Pitilakis K, Anastasiadis A, Pitilakis D, Trevlopoulos K, Senetakis K. Advances in performance-based earth- quake engineering. In: Fardis M, editor. Chapter 6: elastic demand spectra. geotechnical, geological, and earthquake engineering, vol. 13, Part I. Springer; 2010. p. 89–99.
[43] Pitilakis K, Trevlopoulos K, Anastasiadis A, Senetakis K. Seismic response of structures on improved soil. In: Proceedings of the 8th international conference on structural dynamics (EURODYN2011), Leuven, Belgium.
[44] Plimpton S. Fast parallel algorithms for short-range molecular dynamics. J Comput Phys 1995;117(1):1–19.
[45] Potyondy DO, Cundall PA. A bonded-particle model for rock. Int J Rock Mech Min Sci 2004;41(8):1329–64.
[46] Radjai F, Wolf DE, Jean M, Moreau J. Bimodal character of stress transmission in granular packings. Phys Rev Lett 1998;80(1):61–4.
[47] Reddy KR, Saichek RE. Characterization and performance assessment of shredded scrap tires as leachate drainage material in landfills. In: Proceedings of the 14th international conference on solid waste technology and management, Philadelphia, USA.
[48] Rothenburg L, Bathurst RJ. Analytical study of induced anisotropy in idealized granular materials. Géotechnique 1989;39(4):601–14.
[49] Satake M. Fabric tensor in granular materials. In: Vermeer PA, Luger HJ, editors. IUTAM symposium on deformations and failure of granular materials. Rotterdam: Balkema; 1982. p. 63–8.
[50] Schallamach A. Friction and abrasion of rubber. Wear 1958;1(5):384–417.
[51] Senetakis K, Anastasiadis A, Trevlopoulos K, Pitilakis K. Dynamic response of SDOF systems on soil replaced with sand/rubber mixture. In: Proceedings of the ECOMAS thematic conference on computation methods in structural dynamics and earthquake engineering, Rhodes, Greece.
[52] Senetakis K, Anastasiadis A, Pitilakis K. Dynamic properties of sand/rubber (SRM) and gravel/rubber (GRM) mixtures in a wide range of shearing strain amplitudes. Soil Dyn Earthq Eng 2012;33(1):38–53.
[53] Senetakis K, Anastasiadis A, Pitilakis K. The small-strain shear modulus and damping ratio of quartz and volcanic sands. Geotech Test J 2012;35(6). http://dx.doi.org/10.1520/GTJ20120073.
[54] Senetakis K, Coop MR, Todisco MC. Tangential load-deflection behaviour at the contacts of soil particles. Géotech Lett 2013;3(2):59–66.
[55] Senetakis K, Coop MR, Todisco MC. The inter-particle coefficient of friction at the contacts of Leighton Buzzard sand quartz minerals. Soils Found 2013;53(5):746–55.
[56] Senetakis K, Coop MR. The development of a new micro-mechanical inter-particle loading apparatus. Geotech Test J 2014;37(6):1028–39.
[57] Senetakis K, Anastasiadis A. Effects of state of test sample, specimen geometry and sample preparation on dynamic properties of rubber-sand mixtures. Geosynth Int 2015;22(4):301–10.
[58] Shire T, O'Sullivan C, Hanley KJ, Fannin RJ. Fabric and effective stress distribution in internally unstable soils. J Geotech Geoenviron Eng 2014;140(12):04014072.
[59] Simmons G, Brace WF. Comparison of static and dynamic measurements of compressibility of rocks. J Geophys Res 1965;70(22):5649–56.
[60] Simpson B, O'Riordan HJ, Croft DD. A computer model for the analysis of ground movements in London Clay. Géotechnique 1979;29(2):149–75.
[61] Sitharam T, Vinod J, Ravishankar B. Post-liquefaction undrained monotonic behaviour of sands: experiments and DEM simulations. Géotechnique 2009;59(9):739–49.
[62] Thornton C. Numerical simulations of deviatoric shear deformation of granular media. Géotechnique 2000;50(1):43–53.
[63] Uchumira T, Chi N, Nirmalan S, Sato T, Meidani M, Towhata I. Shaking table tests on effect of tire chips and sand mixture in increasing liquefaction resistance and mitigat- ing uplift of pipe. In: Hazarika, Yasuhara, editors. Proceedings, international workshop on scrap tire derived geomaterials—opportunities and challenges, Yokosuka, Japan. p. 179–86.
[64] Valdes JR, Evans MT. Sand-rubber mixtures: experiments and numerical simulations. Can Geotech J 2008;45(4):588–95.
[65] Wei LM, Yang J. On the role of grain shape in static liquefaction of sand-fines mixtures. Géotechnique 2014;64(9):740–5.
[66] Yimsiri S, Soga K. Effects of soil fabric on behaviors of granular soils: microscopic modeling. Comput Geotech 2011;38(7):861–74.
[67] Youwai S, Bergado DT. Strength and deformation characteristics of shredded rubber tire sand mixtures. Can Geotech J 2003;40(2):254–64.
[68] Zornberg JG, Carbal AR, Viratjandr C. Behaviour of tire shred–sand mixtures. Can Geotech J 2004;41(2):227–41.